

# *B* meson decay constants from two-flavor lattice QCD with non-relativistic heavy quarks

A. Ali Khan<sup>1\*</sup>, S. Aoki<sup>2</sup>, R. Burkhalter<sup>1,2</sup>, S. Ejiri<sup>1</sup>, M. Fukugita<sup>3</sup>, S. Hashimoto<sup>4</sup>, N. Ishizuka<sup>1,2</sup>, Y. Iwasaki<sup>1,2</sup>, K. Kanaya<sup>1,2</sup>, T. Kaneko<sup>4</sup>, Y. Kuramashi<sup>4</sup>, T. Manke<sup>1†</sup>, K. Nagai<sup>1</sup>, M. Okawa<sup>4</sup>, H.P. Shanahan<sup>1‡</sup>, A. Ukawa<sup>1,2</sup> and T. Yoshié<sup>1,2</sup>

(CP-PACS Collaboration)

<sup>1</sup> *Center for Computational Physics, University of Tsukuba, Tsukuba, Ibaraki 305-8577, Japan;*

<sup>2</sup> *Institute of Physics, University of Tsukuba, Tsukuba, Ibaraki 305-8571, Japan;*

<sup>3</sup> *Institute for Cosmic Ray Research, University of Tokyo, Kashiwa, Chiba 277-8582, Japan;*

<sup>4</sup> *High Energy Accelerator Research Organization (KEK), Tsukuba, Ibaraki 305-0801, Japan.*

(March 19, 2001)

We present a study of leptonic *B* meson decay constants in lattice QCD with two flavors ( $N_f = 2$ ) of light dynamical quarks using NRQCD for the heavy quark. Gauge configurations are generated with a renormalization-group improved gauge action and a meanfield-improved clover light quark action. Measurements are carried out at two values of  $\beta = 6/g^2$ , each for four sea quark masses, corresponding to the inverse lattice spacing  $a^{-1} \approx 1.3$  and 1.8 GeV in the chiral limit of sea quark. The continuum values of the decay constants are derived by evaluating the discretization errors at each finite lattice spacing. We find  $f_B^{N_f=2} = 204(8)(29)(+44)$  MeV,  $f_{B_s}^{N_f=2} = 242(9)(34)(+38)$  MeV, and  $f_{B_s}^{N_f=2}/f_B^{N_f=2} = 1.179(18)(23)$ , where the errors listed are statistical, systematic and uncertainty due to choice of the physical quantity used to fix the scale. Comparison is made to quenched results ( $N_f = 0$ ) obtained with the same action combination and matching lattice spacings. We find  $f_B^{N_f=2}/f_B^{N_f=0} = 1.07(5)$ ,  $f_{B_s}^{N_f=2}/f_{B_s}^{N_f=0} = 1.10(5)$  and  $(f_{B_s}/f_B)^{N_f=2}/(f_{B_s}/f_B)^{N_f=0} = 1.03(2)$ , which indicates a 5–10% increase in the values of the decay constants, but no appreciable change in the ratio  $f_{B_s}/f_B$ , due to sea quarks.

## I. INTRODUCTION

An accurate determination of the *B* meson decay constant has practical importance, as it is needed, together with the  $\bar{B} - B$  transition matrix elements, for the extraction of the quark mixing matrix elements from the  $\bar{B} - B$  mass difference. To this end much effort has been paid towards a quantitative evaluation of these matrix elements using lattice QCD (for reviews, see [1,2]).

A problem specific to heavy meson calculations with the original lattice formulation is that the heavy quark mass is greater than unity in units of lattice spacing, which makes the lattice artifacts intolerably large. There are two popular formalisms to handle heavy quarks, using the fact that the heavy quark in a *B* meson is non-relativistic, in a way that large discretization effects proportional to the heavy quark mass do not appear. One is the use of the relativistic action with the aid of the non-relativistic reinterpretation (the Fermilab formalism) [3], and the other is simulations with the NRQCD action [4].

The problem with these formalisms, however, is that a continuum extrapolation is not simple. For instance, since the NRQCD action is not renormalizable, an infinite number of terms are involved in the  $aM \rightarrow 0$  limit, and their matching to the continuum theory requires good control of power divergence of the form  $1/(aM)^n$  with  $n$  a positive integer. In the Fermilab formalism the continuum extrapolation is possible in principle, although it is difficult in practice because of a complicated  $a$  dependence of the couplings in the effective Hamiltonian of the heavy quark. Therefore, estimation of systematic errors arising from the continuum extrapolation is a non-trivial task in both formalisms.

\*address till 31 August, 2000

†present address : Department of Physics, Columbia University, New York, NY 10027. U. S. A.

‡present address : Department of Biochemistry and Molecular Biology, University College London, London, England, UK

Another uncertainty in previous calculations of heavy mesons is the effect of dynamical quarks. Most lattice studies to date adopt the quenched approximation. There are two calculations in which dynamical quarks are incorporated (full QCD) [6,7]. The results indicate that the inclusion of dynamical quarks increases the value of  $f_B$  and  $f_{B_s}$ . The study by Collins *et al.* [6], using NRQCD for heavy quark and the clover action for light valence quarks, however, has been made only at a single lattice spacing in a small physical volume, and with the Kogut-Susskind staggered action for sea quarks with a mass around that of the strange quark. The other study by the MILC Collaboration [7], while covering a range of lattice spacings and sea quark masses, uses the Wilson action both for heavy and light valence quarks, but employs the staggered action for sea quarks. The problem with these calculations are that the actions for valence and sea quarks are different, having different symmetry structures at finite lattice spacings. This would be an additional source of systematic errors.

We study the  $B$  meson decay constants,  $f_B$  and  $f_{B_s}$ , incorporating two flavors of light dynamical quarks, which are identified as  $u$  and  $d$  quarks. The strange quark is treated in the quenched approximation. In order to test the estimation of systematic errors in the final results in the continuum limit, we compare the results from the two heavy quark formalisms. The work with the Fermilab formalism has been published separately [5]. In this paper, we present the calculation using NRQCD.

We carry out full QCD calculation with a consistent use of a quark action for both sea and light valence quarks. We adopt a renormalization group improved gauge action [8] for the gluon sector and an  $O(a)$ -improved clover action [9] for sea and light valence quarks [10–12]. The use of the improved action enables us to reduce discretization errors, and makes it possible to study decay constants at moderate lattice spacing, which is feasible with the present computer resource.

The full QCD calculation is performed at two lattice spacings ( $1/a \simeq 1.3$  and  $1.8$  GeV). In order to study the dynamical quark effects, we perform parallel quenched simulations with the same action, tuning the lattice spacing to be the same as those in full QCD simulations.

The outline of this paper is as follows. In Sec. II, we introduce the lattice formulations of NRQCD used in this calculation, and define the operators that contribute to the axial vector current. Simulation details, such as the run parameters and choice of operators, and fitting methods are described in Sec. III. In Sec. IV, we discuss determinations of the physical lattice spacing, the  $B$  meson masses and decay constants. A detailed discussion on the extrapolation and interpolation to the physical quark masses is given. We then attempt to obtain the continuum results by estimating the discretization errors at each finite lattice spacing in Sec. V. A comparison with results of previous studies is made in Sec. VI, and the conclusions are given in Sec. VII. Detailed numerical results are collected in the Appendix.

## II. FORMALISM

### A. Actions

For gluons we adopt a renormalization-group (RG) improved gauge action consisting of plaquettes and  $1 \times 2$  rectangular Wilson loops [8]. The action for both sea quarks and light valence quarks is taken to be the  $O(a)$ -improved clover action [9] with a meanfield-improved clover coefficient  $c_{SW} = P^{-3/4}$ , where the plaquette  $P$  is evaluated in one-loop perturbation theory as  $P = 1 - 0.8412/\beta$ . For our choice of parameters the measured values of plaquette  $\langle P \rangle$  is well approximated by the one-loop evaluation [12].

For the heavy quarks we use NRQCD corrected to  $O(1/M_0)$  with  $M_0$  the heavy quark mass. Previous quenched NRQCD calculations have shown that  $O(1/M_0^2)$  corrections are small in the decay constants, being of the order of  $\sim 3 - 4\%$  at the lattice spacings used in this study [13–15]. There are various ways to discretize an NRQCD action (see *e.g.*, [4,14,16]). Here, we choose the action that is symmetric under a time reversal transformation:

$$S_{NRQCD} = \sum \psi_t^\dagger \left[ \psi_t - \left(1 - \frac{a\delta H}{2}\right)_t \left(1 - \frac{aH_0}{2n}\right)_t U_4^\dagger \left(1 - \frac{aH_0}{2n}\right)_{t-1} \left(1 - \frac{a\delta H}{2}\right)_{t-1} \psi_{t-1} \right], \quad (1)$$

where  $\psi_t$  is a two-component Pauli spinor at a time slice  $t$ . The sum runs over all lattice sites, while indices to represent spatial positions are suppressed. The operators  $H_0$  and  $\delta H$  correspond to the non-relativistic kinetic energy and the spin-chromomagnetic interaction, as defined by

$$H_0 \equiv -\frac{\Delta^{(2)}}{2M_0}, \quad (2)$$

$$\delta H \equiv -c_B \frac{g}{2M_0} \vec{\sigma} \cdot \vec{B}, \quad (3)$$

respectively, where  $\Delta^{(2)}$  is a Laplacian discretized in a standard way and  $\vec{B}$  represents a chromomagnetic field strength defined with a clover-leaf shape as in [4]. The stabilization parameter  $n$  is introduced to avoid an instability of the Green function at large separation due to high-momentum modes. In the free theory, this parameter should satisfy  $n > 3/(2aM_0)$  [4]. We choose a larger value of  $n$  to make the simulation stable [14,15]. The actual numbers are given in Table I for full and in Table II for quenched QCD runs. Gauge links appearing in the NRQCD action are meanfield-improved,  $U_\mu \rightarrow U_\mu/u_0$ , with  $u_0$  determined from the mean link in Landau gauge. The coefficient  $c_B$  is set to its tree-level value, *i.e.* unity. We let the heavy quark Green functions to evolve from  $t=0$  to  $T/2$ , and a time reversed evolution through the second half of the lattice from the same source.

## B. Current operators

The pseudoscalar decay constant is defined by

$$if_{BP\mu} = \langle 0|A_\mu|B(p)\rangle, \quad (4)$$

where the axial current  $A_\mu = \bar{q}\gamma_5\gamma_\mu h$  is formed with the relativistic spinors  $q$  for the light quark and  $h$  for the heavy quark. We restrict our considerations to the time component,  $A_0$ .

The heavy quark field  $h$  is related to a non-relativistic field  $Q$  via a Foldy-Wouthuysen-Tani transformation at the tree level. Ignoring the  $O(1/M^2)$  terms, this reads

$$h = \left(1 - \frac{\vec{\gamma} \cdot \vec{\nabla}}{2M_0}\right) Q, \quad (5)$$

where

$$Q = \begin{pmatrix} \psi \\ 0 \end{pmatrix}. \quad (6)$$

We write the two lattice operators contributing to the time component of the heavy-light axial vector current as

$$\begin{aligned} J_L^{(0)} &= \bar{q}\gamma_5\gamma_0 Q, \\ J_L^{(1)} &= -\frac{1}{2M_0}\bar{q}\gamma_5\gamma_0\vec{\gamma} \cdot \vec{\nabla} Q. \end{aligned} \quad (7)$$

In matching the continuum operator to the lattice counterparts, an additional operator  $J_L^{(2)}$  appears at  $O(1/M)$

$$J_L^{(2)} = \frac{1}{2M_0}\bar{q}\vec{\gamma} \cdot \overleftarrow{\nabla} \gamma_5\gamma_0 Q, \quad (8)$$

though its matrix element is equal to that of  $J_L^{(1)}$  at zero momentum due to translational invariance on the lattice. Thus, at the one-loop level we use

$$A_0 = (1 + \alpha_s\rho_A^{(0)})J_L^{(0)} + (1 + \alpha_s\rho_A^{(1)})J_L^{(1)} + \alpha_s\rho_A^{(2)}J_L^{(2)}, \quad (9)$$

where  $\rho_A^{(0)}$ ,  $\rho_A^{(1)}$  and  $\rho_A^{(2)}$  have been computed in Ref. [17]<sup>1</sup> for the RG-improved gauge action. The coefficient  $\rho_A^{(2)}$  diverges in the limit of  $aM_0 \rightarrow \infty$  as  $0.34 \times 2aM_0$ , which cancels the factor  $1/M_0$  in the definition of  $J_L^{(2)}$  and gives a finite contribution. This remaining contribution corresponds to the improvement of discretization error of  $O(\alpha_s a)$  [18] in the static limit.

For  $\alpha_s$ , we use the coupling defined with the  $\overline{MS}$  scheme at  $\mu = 1/a$ , which is evaluated using the one-loop relation

$$\frac{1}{g_{\overline{MS}}^2(\mu)} = \frac{(c_0 P - 8c_1 R)\beta}{6} - 0.1006 + \frac{22}{16\pi^2} \log(\mu a) + N_f \left(0.03149 - \frac{4}{48\pi^2} \log(\mu a)\right). \quad (10)$$

The meanfield improvement is applied using measured values of the  $1 \times 1$  and  $1 \times 2$  Wilson loops,  $P$  and  $R$ .

---

<sup>1</sup> The definition of the lattice currents  $J_4^{(i)}$  in [17] is slightly different from  $J_L^{(i)}$  used in this paper. The tree level rotation is included in  $J_4^{(0)}$  in [17]. The one-loop coefficients  $\rho_A^{(i)}$  are modified accordingly.

### III. SIMULATION DETAILS

#### A. Gauge configurations

The CP-PACS Collaboration has generated a set of full QCD gauge configurations incorporating two flavors of light dynamical quarks at four values of gauge coupling,  $\beta = 1.8, 1.95, 2.1, 2.2$ , using the Hybrid Monte Carlo (HMC) algorithm [10–12]. At each  $\beta$ , four sea quark masses  $m_{sea}$  are chosen in the range  $0.5m_s \lesssim m_{sea} \lesssim 3m_s$ , where  $m_s$  denotes the strange quark mass. In the chiral limit of sea quarks, these couplings correspond to lattice spacings  $a$  with  $1 \text{ GeV} \lesssim a^{-1} \lesssim 2.2 \text{ GeV}$ . The spatial lattice size is about 2.5 fm at  $\beta = 1.8, 1.95$  and 2.1, while it is about 1.9 fm at  $\beta = 2.2$ . The parameters of the configurations are summarized in the left half of Table III.

In the present study we use the configurations at  $\beta = 1.95$  ( $a^{-1} \simeq 1.3 \text{ GeV}$ ) and 2.1 ( $a^{-1} \simeq 1.8 \text{ GeV}$ ); the entire gauge configurations we generated are analyzed at  $\beta = 1.95$ , whereas half the configurations, corresponding to the first 2000 trajectories, are employed for  $\beta = 2.1$ . The configurations are separated by 10 HMC trajectories at  $\beta = 1.95$  and by 5 trajectories at 2.1. We discard configurations at  $\beta = 1.8$ , because of expected large discretization errors, and at  $\beta = 2.2$  for a too small physical volume. Details of the parameters employed in our analysis are listed in Table I.

The CP-PACS study of full QCD is supplemented by quenched simulations. These simulations are based on a set of quenched configurations with the same gauge action separated by 100 sweeps, each sweep consisting of 1 heatbath and 4 overrelaxation steps. The gauge couplings in the quenched configurations are tuned such that the string tension matches the one in full QCD at four sea quark masses in our simulation and at the physical sea quark mass point corresponding  $u$  and  $d$  quarks, as shown in the right half of Table III [5]. We analyze a subset of the quenched configurations at four values of  $\beta$  as listed in Table II. The first two values ( $\beta = 2.187$  and 2.281) correspond to the full QCD runs with the heaviest and the lightest sea quark masses at  $\beta = 1.95$ . The third ( $\beta = 2.334$ ) and the fourth, ( $\beta = 2.575$ ), correspond to full QCD at  $\beta = 1.95$  and 2.1 at the physical sea quark mass, respectively. Details of the parameters of these quenched runs are given in Table II.

#### B. Correlator measurements

In order to improve the overlap of interpolating field with the heavy-light meson ground state, we use smeared operators  $O_S$

$$O_S(\vec{x}, t) = \sum_{\vec{y}} \bar{q}(\vec{x}, t) \gamma_5 Q(\vec{y}, t) \phi(|\vec{x} - \vec{y}|), \quad (11)$$

on the gauge configurations fixed to the Coulomb gauge. For the smearing function  $\phi(|\vec{x} - \vec{y}|)$  we use an exponential form,

$$\begin{aligned} \phi(|\vec{x} - \vec{y}|) &= A \exp(-B|\vec{x} - \vec{y}|) \quad \text{for } |\vec{x} - \vec{y}| \neq 0 \\ \phi(0) &= 1. \end{aligned} \quad (12)$$

We calculate correlators using smeared operators at the source and using both local and smeared operators at the sink,

$$\begin{aligned} C_{SS}(t) &= \sum_{\vec{x}} \langle O_S(\vec{x}, t) O_S^\dagger(\vec{0}, 0) \rangle, \\ C_{SL}(t, |\vec{p}|) &= \sum_{\vec{x}} e^{i\vec{p} \cdot \vec{x}} \langle O_L(\vec{x}, t) O_S^\dagger(\vec{0}, 0) \rangle, \end{aligned} \quad (13)$$

where  $O_L$  denotes a local pseudoscalar density. The spatial momentum  $\vec{p}$  is introduced for  $C_{SL}$  to study the energy-momentum dispersion relation of mesons. We make measurements for momenta  $p^2 = |\vec{p}|^2 = 0, 1, \dots, 5$  in units of  $(2\pi/La)^2$  with  $L$  the spatial extent of the lattice. We average over all possible spatial directions.

The correlators for the axial currents are given by

$$C_{SL}^{(i)}(t) = \sum_{\vec{x}} \langle J_L^{(i)}(\vec{x}, t) O_S^\dagger(\vec{0}, 0) \rangle, \quad i = 0, 1, 2. \quad (14)$$

Note that  $C_{SL}^{(0)}(t) \equiv C_{SL}(t, \vec{0})$  since the lower two components of  $Q$  vanish.

### C. Correlator fits

To calculate the decay constants we need the amplitude of the local currents. Since smeared-smeared and smeared-local correlators both have the exponential falloff with the same exponent controlled by  $E_{sim}$ , we make a simultaneous fit to a single exponential as

$$C_{SS}(t) = Z_S^2 \exp(-E_{sim}t), \quad (15)$$

$$C_{SL}^{(i)}(t) = Z_L^{(i)} Z_S \exp(-E_{sim}t), \quad i = 0, 1, 2. \quad (16)$$

We apply a bootstrap procedure with 500 samples, taking correlations between different correlators and time slices into account. For the dynamical configurations, we bin over 2 configurations at  $\beta=1.95$  and 5 configurations at  $\beta=2.1$ . The quenched configurations are regarded as independent and are not binned. Results from forward and time reversed evolution on the same configurations are always averaged. In the full QCD analysis at  $\beta=2.1$  we introduce a cutoff on the ratio of the largest to the smallest eigenvalues of the covariance matrix to avoid a low value of the goodness-of-fit  $Q$ . We have checked for the heaviest and the lightest sea quark mass that the effect of this procedure on the decay constants is small, amounting to at most  $\sim 25\%$  of the statistical error. The problem of a low  $Q$  at  $\beta=2.1$  might arise from the smaller number of independent configurations.

The fitting interval  $[t_{min}, t_{max}]$  is chosen such that both correlators already reach a plateau at  $t_{min}$ . This is judged by  $Q$ , as well as by eye from the effective mass and effective amplitude plots. Correlators, in particular  $C_{SS}$ , are often dominated by noise for large  $t$ , which is indicated by a decrease of  $Q$  for a large  $t_{max}$ . We cut the fit at  $t_{max}$  before noise dominates.

Examples of the effective mass plots for  $C_{SL}^{(0)}$  and  $C_{SS}$  are shown in Figs. 1 and 2, where the light valence quark mass is taken approximately to be the strange quark mass and the heavy quark mass to be the  $b$  quark. In Fig. 1 the upper two panels illustrate full QCD data at  $\beta=1.95$  with the lightest sea quark mass, and the lower two show quenched results at  $\beta=2.334$  corresponding to the physical value of the sea quark mass in full QCD at  $\beta=1.95$ . Figure 2 shows similar plots at  $\beta=2.1$ .

Energy for a given finite spatial momentum  $E_{sim}(p^2)$  is extracted from the difference  $\Delta E(p^2) \equiv E_{sim}(p^2) - E_{sim}(0)$  using a single exponential fit to the ratio

$$\frac{C_{SL}(t, |\vec{p}|)}{C_{SL}(t, |\vec{0}|)} = A(|\vec{p}|) \exp(-\Delta E(p^2)t). \quad (17)$$

An example of the effective mass is shown in Fig. 3 for full QCD simulations at  $\beta=2.1$ .

## IV. ANALYSIS

### A. Fixing the physical scale

We carry out a partially quenched analysis of the dynamical configurations. Namely, we evaluate the decay constants for the configurations at each sea quark mass, at which the lattice spacing and physical quark masses are determined by varying the valence light quark mass as we do in the quenched analysis. We then extrapolate the results to the physical value of the sea quark mass. In this subsection we discuss the determination of the lattice scale.

In simulations of full QCD with the realistic spectrum of dynamical sea quarks, one should in principle obtain a unique value for the lattice spacing  $a$  from any physical quantity it is determined. In our simulation, however, we obtain different values of  $a$  depending on the quantity used to fix the scale since dynamical quark effects other than those of  $u$  and  $d$  quarks are not included.

One way to determine the lattice spacings is to use the  $\rho$  meson mass. We refer the reader to Ref. [10–12] for the light hadron spectroscopy calculation, from which we constructed Tables IV and V.

Another way is to use  $\Upsilon$  level splittings. Specifically, we take the spin-averaged  $1P-1S$  splitting, which is considered to be relatively insensitive to systematic errors. Our study of the  $\Upsilon$  spectroscopy using the NRQCD action is described in Ref. [19].

One may think that the most natural scale for the physics of  $B$  mesons is their level splittings. In quenched studies [20,21], it was found that the scale from the spin-independent  $B$  spectrum agrees with that from the  $\rho$  meson mass. We defer a verification in full QCD to a separate work. In this study, we study the scale from the  $\rho$  meson mass, denoted as  $a_\rho$  in the followings, and that from the  $\Upsilon$   $1P-1S$  splitting, denoted as  $a_\Upsilon$ . We do not adopt the string tension to fix the scale because its physical value is not well known.

Our results for the Lattice spacings are listed in Tables IV and V for unquenched and quenched lattices respectively. Note that  $a_\rho$  given in this paper differs slightly from the one presented in Ref. [19], the latter being calculated in the chiral limit where the  $(u, d)$  quark mass vanishes rather than at the physical point. The ratio of the scales is plotted in Fig. 4 for quenched (open symbols) and full (filled symbols) QCD. The ratio becomes closer to unity with inclusion of the dynamical quark, but the discrepancy still remains significant. We note that the discrepancy does not decrease towards the continuum limit.

The light quark mass corresponding to the  $u, d$  quarks is determined from  $m_\pi$ . To determine the strange quark mass, we use either the  $K$  meson mass or the  $\phi$  meson mass. The corresponding hopping parameters denoted by  $K_l$ ,  $K_s(K)$  and  $K_s(\phi)$ , are given in Tables IV and V.

## B. $B$ meson masses

In NRQCD, the exponential falloff of the correlator in Euclidean time,  $E_{sim}$ , represents the bare binding energy. We expect that the nonperturbative mass of heavy-light mesons is inferred from the meson dispersion relation. We use the relativistic form

$$\Delta E(p^2) \equiv E_{sim}(p^2) - E_{sim}(0) = \sqrt{M_{kin}^2 + p^2} - M_{kin}. \quad (18)$$

In practice, we determine this energy difference from a fit of the ratio of the correlators at  $p^2 = (2\pi/La)^2$  and  $p^2 = 0$  to a single exponential. The results are given in Table X for full QCD and in Table XI for the quenched case in the Appendix. We also examine this particular form of the dispersion relation by comparing the results using momenta larger than one lattice unit, and find that they agree within errors. An example for  $M_{kin}$  as a function of  $p^2$  is given in Fig. 5 for a quenched lattice at  $\beta = 2.575$ .

The meson masses can also be estimated from  $E_{sim}$ , through the perturbative relation

$$M_{pert} = E_{sim} + \Delta_{pert} \equiv E_{sim} + Z_m M_0 - E_0, \quad (19)$$

where  $Z_m$  is the quark mass renormalization constant, and  $E_0$  is a shift of the zero point of the energy that occurs in non-relativistic and static theories. We employ one-loop perturbative values of  $Z_m$  and  $E_0$  [17], using  $\alpha_{\overline{MS}}$  as defined in (10) at the scale  $1/a$ . Results for  $E_{sim}$  are given in Tables XII and XIII, and those for  $M_{pert}$  in Tables XIV and XV in the Appendix.

The statistical errors in  $E_{sim}$  are very small. The error of  $M_{pert}$  quoted in these tables is dominated by the systematic error from higher order radiative corrections, as estimated by  $\alpha_{\overline{MS}}^2(1/a)$  times the meson mass. We find that the one-loop contribution to  $\Delta_{pert}$  is always smaller than our estimate of the two-loop error, which increases our confidence in the error estimate.

For light valence quark masses around  $m_s$ ,  $M_{kin}$  and  $M_{pert}$  agree within the combined errors for all configurations except for those for  $\beta = 2.1$ ,  $K_{sea} = 0.1357$  in full QCD, and for  $\beta = 2.575$  in quenched QCD. Even for these cases the difference is at most 2 standard deviations of the statistical error in  $M_{kin}$ . In Fig. 6 we show a comparison between  $M_{kin}$  and  $M_{pert}$  for full (top panel) and quenched QCD (bottom panel) at our finest lattice spacing of  $a_\rho^{-1} \approx 1.8$  GeV. The full QCD data show an agreement which is typical of our data, while for the quenched data we show the case of the largest discrepancy.

To determine the bare  $b$  quark mass,  $M_{0b}$ , we employ the kinetic meson mass  $M_{kin}$ , as it is free from higher order perturbative errors. The systematic uncertainty in the choice of the method will be discussed later. We first fit the mass as a linear function of the light quark mass,

$$M = A_q + \frac{B_q}{2} \left( \frac{1}{K} - \frac{1}{K_c} \right), \quad (20)$$

and extrapolate or interpolate to the physical value  $K_l$  and  $K_s$  to obtain the heavy-light meson masses  $M_l$  and  $M_s$ . The result is then expressed as a function of the heavy quark mass, as

$$M_{l,s} = A_Q M_0 + B_Q, \quad (21)$$

and  $M_{0b}$  is determined by requiring  $M_l$  or  $M_s$  to equal the physical meson mass,  $M_B$  or  $M_{B_s}$ , respectively.

Examples for these fits in the light and heavy quark mass are given in Fig. 7. On the right panel, a plot of  $M_s/M_0$  is shown as a function of  $1/M_0$ , which is  $A_Q + B_Q/M_0$ . Results using the  $B$  meson agree with those from  $B_s$  allowing for larger errors. We use the  $B_s$  rather than the  $B$  meson to calculate the central values of  $M_{0b}$  to avoid the larger

statistical and possible systematic errors from the extrapolation to  $K_l$ . The difference between the use of the  $K$  and  $\phi$  mesons to fix the strange quark mass is negligible compared to other errors in heavy-light meson mass. We take the central value from the  $K$  meson. The numerical results for  $M_{0b}$  are listed in Table XVI (full) and in Table XVII (quenched).

### C. Decay constants

The decay constants are calculated from the results of the fit (15) and (16) according to

$$a^{3/2}(f\sqrt{M})^{(i)} = \frac{1}{\sqrt{M}} \langle 0 | J_L^{(i)} | P(\vec{0}) \rangle = \sqrt{2} Z_L^{(i)} \sqrt{1 - \frac{3K}{4K_c}}, \quad (22)$$

where  $|P(\vec{0})\rangle$  denotes a pseudoscalar heavy-light meson state of mass  $M$  at rest. The normalization factor  $\sqrt{1 - \frac{3K}{4K_c}}$  for the light quark field in (22) is motivated by the meanfield improvement of the perturbative renormalization factor [22], with which the one-loop coefficient  $\rho_A^{(0)}$  in (9) is modified. The lattice results for the matrix elements  $(f\sqrt{M})^{(0)}$  and  $(f\sqrt{M})^{(1)}$  are listed in Tables XVIII–XIX for full QCD and in Tables XX–XXIII for quenched QCD. As mentioned before in Sec. II B,  $(f\sqrt{M})^{(2)} = (f\sqrt{M})^{(1)}$  at zero momentum.

The physical decay constant is then obtained, following (9), by

$$f\sqrt{M} = (1 + \alpha_s \rho_A^{(0)})(f\sqrt{M})^{(0)} + (1 + \alpha_s \rho_A^{(1)})(f\sqrt{M})^{(1)} + \alpha_s \rho_A^{(2)}(f\sqrt{M})^{(2)}. \quad (23)$$

The one-loop corrections of the different currents contribute with different signs and partially cancel each other. As shown in Fig. 8 as an example for full QCD, the relative contribution of each of these corrections to the whole decay matrix element  $f\sqrt{M}$  is small. The largest is the correction to  $(f\sqrt{M})^{(0)}$ , being of the order of a few percent. The overall one-loop correction is 3 – 6% for the dynamical case, and 3 – 5% for quenched. The one-loop correction for the RG-improved gauge action is thus smaller than for the plaquette gauge action for which the correction amounts to roughly 10% (see e.g. [14,15]).

### D. Analysis of heavy and light quark mass dependence

We find that the decay matrix elements  $a^{3/2}(f\sqrt{M})^{(i)}$  are well described by a linear function in the light quark mass  $1/(2K) - 1/(2K_c)$  as shown in Fig. 9 (top panel). Using the linear fit, we interpolate the data to  $K_s$  or extrapolate to  $K_l$ . Then, we make a quadratic fit in  $1/M_0$  and interpolate to the  $b$  quark mass,  $1/M_{0b}$ . Figure 9 (bottom) shows this fit for full QCD on the finest lattice.

For quenched QCD this completes the analysis of the decay constant. We give the renormalized decay constants in Table VI.

For full QCD we carry out this procedure separately for each sea quark mass  $m_{sea}$ , using partially quenched values for the lattice spacing and  $K_c$ ,  $K_l$  and  $K_s$ . The resulting renormalized decay constants are given in Table VII. From these data we calculate the physical decay constants by extrapolating the sea quark mass to the  $u, d$  quark mass. We use a linear fit in  $(am_\pi)^2$ , where  $m_\pi$  is the pion mass of the sea quark. The sea quark mass dependence of  $f_B$ ,  $f_{B_s}$ , and  $f_{B_s}/f_B$ , is very mild. On finer lattices, there is a slight upwards shift of the decay constants as the sea quark mass is decreased. In Fig. 10, this is demonstrated for  $f_B$  at  $\beta = 2.1$ . The final results for full QCD are given in Table VIII.

We note that the decay constants we obtained for finite lattice spacings agree very well with those from the Fermilab formalism [5] for both quenched and full calculations.

We add comments on possible systematic errors from various steps of the analysis procedure: (i) The bare  $b$  quark mass using the  $\rho$  mass to set the scale is slightly higher than that from the  $\Upsilon$ , but the two agree within statistical errors. (ii) The statistical error on the mass is included within the bootstrap procedure. There is a good agreement between results from  $M_{kin}$  and  $M_{pert}$ , and if the perturbative error is included in the determination using  $M_{pert}$ , their errors are very similar. We take results obtained with the kinetic masses for our central values. (iii) An alternative method to represent the heavy quark dependence of  $f^{(i)}\sqrt{M}$  is to employ the heavy-light meson mass instead of the heavy quark mass. This circumvents the determination of  $M_{0b}$ . The results agree with those using  $M_{0b}$  within the statistical errors, which are similar in magnitude in both methods. We quote the numbers from the procedure using  $M_{0b}$  as our central values.

## V. ESTIMATE OF CONTINUUM RESULTS

While discretization errors decrease as the lattice spacing becomes smaller, the  $1/M$  operators introduce radiative corrections that go as powers of  $1/a$  in NRQCD. Thus NRQCD breaks down in the limit of vanishing lattice spacing, and we cannot perform a continuum extrapolation as a matter of principle. The aim is rather to find a range of lattice spacings where the result is approximately independent of the cutoff with small systematic errors.

We have plotted the resulting  $f_B$  and  $f_{B_s}$  at finite lattice spacing in Fig. 11 and 12 for both quenched and full QCD calculations, where statistical errors are shown with thick bar symbols. We see the data for quenched QCD (top panels) exhibiting a signature for a plateau for  $a_\rho \leq 0.8 \text{ GeV}^{-1}$ . The data for full QCD calculation however show a sizable drop from  $a_\rho = 0.79$  to  $0.56 \text{ GeV}^{-1}$ . Nevertheless, it is perhaps possible to estimate the continuum value if we can properly estimate the discretization error at each lattice spacing, and we consider this problem in the following.

The leading systematic errors due to finite lattice spacings are  $O(\alpha_s a \Lambda_{QCD})$  and  $O(a^2 \Lambda_{QCD}^2)$  with the clover action for light valence quarks. In the NRQCD heavy quark action, the tree level matching of the chromomagnetic coupling  $c_B$  leads to the error of  $O(\alpha_s \Lambda_{QCD}/M_b)$ . We also expect the discretization error of  $O(\Lambda_{QCD} a/M_b)$  from the NRQCD action. Since the matching calculation of the axial current has been made in one-loop perturbation theory, we expect an  $O(\alpha_s^2)$  radiative correction. In addition, there is an  $O(\alpha_s^2/(aM_b))$  term, which is formally subleading compared to the  $O(\alpha_s^2)$  term, but still gives one of the leading  $1/a$  contributions. An  $O(\Lambda_{QCD}^2/M_b^2)$  contribution comes from the neglected  $1/M^2$  corrections to the NRQCD Lagrangian. In Table IX we list an estimate of the systematic errors for  $f_B$  and  $f_{B_s}$  on our lattices. We use  $\alpha_{\overline{MS}}(1/a)$  for the coupling constant  $\alpha_s$ . For the typical momentum scale  $\Lambda_{QCD}$ , we naively expect that its order is around 200-300 MeV. In this analysis, however, we take a value which is larger by a factor two and use  $\Lambda_{QCD} = 600 \text{ MeV}$ , in order to make the estimate more conservative. The overall error is calculated by summing the individual contributions in quadrature.

In Figs. 11 and 12 the discretization errors thus estimated are shown with thin error bars. Looking first at figures for the quenched case (top panels) we see that the ranges of error bars overlap among all data points, but also that the value of plateau is within the ranges of error bars. Therefore, we consider that the continuum value of the quenched decay constant is located within the estimated errors. We take the data at the weakest coupling, with which the error estimate becomes minimum,

$$f_B^{N_f=0} = 191 \pm 4 \pm 27 \text{ MeV}, \quad (24)$$

$$f_{B_s}^{N_f=0} = 220 \pm 4 \pm 31 \text{ MeV}, \quad (25)$$

as our estimate for the continuum value, where the first error is statistical, and the second is uncertainty associated with the discretization. These values are shown by horizontal lines in the figure. The errors here do not include systematic errors from the uncertainties of the strange quark mass (3%) and the lattice scale which exceeds 30% (see Fig. 4). The error due to strange quark mass is ascribed to both lattice artifacts and quenching effects. As seen in Table VI this uncertainty decreases towards weaker couplings. On the other hand, the uncertainty due to lattice scale does not diminish from strong to weaker couplings.

For the full QCD case, we could not see a plateau within the statistical errors in Figs. 11 and 12. From the same reasoning as in the quenched case, however, we expect that the continuum value is within the error range when we include systematic errors. Indeed, the final error bars of the two data points largely overlap in Figs. 11 and 12. Taking the data with a smaller error bar (*i.e.* at the weaker coupling), we have

$$f_B^{N_f=2} = 204 \pm 8 \pm 29 \text{ MeV}, \quad (26)$$

$$f_{B_s}^{N_f=2} = 242 \pm 9 \pm 34 \text{ MeV}, \quad (27)$$

as our ‘final’ estimate. We take these value as still provisional, since a plateau is not identified within the statistical errors. In full QCD, the uncertainty from the strange quark mass is about 1%. The uncertainty from the lattice scale is 22% in full QCD, which is smaller than that in the quenched case, but is still substantial (see Fig. 14). To be conservative we add this error to the final estimate of errors for the decay constants.

Figure 13 shows a similar analysis for the ratio  $f_{B_s}/f_B$ . This ratio is rather insensitive to the perturbative corrections and the heavy quark action. The dominant errors come from the light quark action, *i.e.*  $O(\alpha_s a \Lambda_{QCD})$  and  $O(a^2 \Lambda_{QCD}^2)$ . We estimate the systematic error of  $f_{B_s}/f_B - 1$  by quadrature. We find the systematic error to be smallest again at the finest lattice spacing, whose results are therefore taken as our final estimates. We obtain

$$\left( \frac{f_{B_s}}{f_B} \right)^{N_f=0} = 1.150 \pm 0.009 \pm 0.020, \quad (28)$$

$$\left( \frac{f_{B_s}}{f_B} \right)^{N_f=2} = 1.179 \pm 0.018 \pm 0.023. \quad (29)$$



To study the effect of dynamical sea quarks, we take the ratio of unquenched to the quenched results. We expect that most systematic errors cancel, and we obtain,

$$\frac{f_B^{N_f=2}}{f_B^{N_f=0}} = 1.07(5); \quad (30)$$

$$\frac{f_{B_s}^{N_f=2}}{f_{B_s}^{N_f=0}} = 1.10(5); \quad (31)$$

$$\frac{(f_{B_s}/f_B)^{N_f=2}}{(f_{B_s}/f_B)^{N_f=0}} = 1.03(2). \quad (32)$$

where only the statistical errors are retained. We observe that the inclusion of dynamical sea quarks increases the decay constants, as noted in [6,7]. The effects are 1.5 sigma for  $f_B$ , and 2 sigma for  $f_{B_s}$ .

## VI. COMPARISON WITH OTHER STUDIES

We first note that the decay constants we obtained with the NRQCD formalism agree very well with those obtained using the Fermilab formalism;  $f_B = 188 \pm 3 \pm 26$  MeV and  $f_{B_s} = 220 \pm 2 \pm 31$  MeV from a quenched calculation, and  $f_B = 208 \pm 10 \pm 29$  MeV and  $f_{B_s} = 250 \pm 10 \pm 35$  MeV from a full QCD calculation [5]. This justifies the validity of the two formalisms within the statistic and systematic errors.

We now compare our quenched calculation to the previous NRQCD results, [14] and [15], and to a quenched world average [1] in Fig. 15. In Ref. [14], marked as GLOK in Fig. 15, the clover light quark action is used with a tree-level meanfield-improved clover coefficient, and the NRQCD action includes  $1/M^2$  corrections at the tree-level. The lattice spacing, fixed from  $m_\rho$ , is  $a^{-1} \simeq 2$  GeV. The calculation of the JLQCD Collaboration [15] employed the clover light quark action with a meanfield-improved one-loop clover coefficient, and heavy quarks with NRQCD corrected through  $O(1/M)$ . The scaling of the decay constant is tested at three lattice spacings, and the central value is extracted from runs at a lattice spacing  $a^{-1} \simeq 1.6$  GeV, with the string tension used to set the scale. The scaling test is also made for  $f_{B_s}$  in Ref. [24] in the range  $a^{-1}=1.1$  to 2.6 GeV. For the world average, we use the value quoted in Ref. [1] that includes a variety of quark actions. Our value (labeled as “this work”) is slightly higher than those of JLQCD and the world average by 1.5 sigma. Our value, however, disagrees with the GLOK result by 2.5-3 sigma.

In Fig. 16, we compare our result from two-flavor QCD with other dynamical calculations that use the plaquette gauge action. Ref. [6] denoted as SGO uses the NRQCD action corrected through  $O(1/M)$  for the heavy quark and a tree-level clover action for the light valence quark. The calculation used a set of dynamical gauge configurations with staggered quarks at a mass around the strange quark mass, but on a somewhat small physical volume ( $L_s \sim 1.6$  fm). The lattice spacing ( $a^{-1} \simeq 2$  GeV) is fixed with  $m_\rho$ . The result from MILC [7] is an ongoing study using two flavors of staggered sea quarks, and both Wilson and (fat-link) clover action for valence quarks. The lattice spacings are set using  $f_\pi$ , and the central value is extracted from the continuum extrapolation of the Wilson results. Our result is again slightly higher, but agrees with the others within one sigma error.

## VII. CONCLUSIONS

We have calculated the  $B$  meson decay constants in two-flavor full QCD using the  $O(1/M)$  NRQCD action, paying attention to the sea quark mass dependence and extrapolation to the chiral limit of the sea quark as well as estimates of discretization errors. We have used improved actions for both quarks and gluons to minimize the discretization error at a modest lattice spacing. We also have performed quenched simulations at matching lattice spacings using the same actions, to study the effect of dynamical sea quarks.

We have confirmed a plateau in the plot of the decay constants as a function of lattice spacing for the quenched calculation, but could not see a plateau in the full QCD calculation, within the statistical errors. We have estimated the decay constant in the continuum by evaluating systematic errors from discretization at each lattice spacing.

We have found that the NRQCD action and the relativistic Fermilab formalism give consistent estimates for the  $B$  meson decay constants. Our values of  $f_B$  and  $f_{B_s}$  are slightly higher than those from previous studies, but the disagreement is at most at 1 sigma level.

We have confirmed that the sea quark effect makes the decay constants larger by  $\approx 10\%$ , which is about 1.5–2 sigma effects in our statistics. The systematic error due to the uncertainty of the strange quark mass (whether it is

determined from  $K$  or  $\phi$ ) is reduced to a negligible level by the introduction of two flavors of dynamical sea quarks. Comparing the results using the lattice scales from the  $\rho$  meson mass and the  $\Upsilon$  mass splitting, we find that the uncertainty from the lattice scale is also smaller in full QCD, but remains to give a substantial error to the decay constants.

Our final result for the decay constant is summarized as,

$$f_B^{N_f=2} = 204 \pm 8 \pm 29^{+44}_{-0} \text{ MeV}; \quad (33)$$

$$f_{B_s}^{N_f=2} = 242 \pm 9 \pm 34^{+38}_{-0} \text{ MeV}; \quad (34)$$

$$\frac{f_{B_s}^{N_f=2}}{f_B^{N_f=2}} = 1.179 \pm 18 \pm 23, \quad (35)$$

where the central values are taken from those using the lattice scale from the  $\rho$  meson mass, because the  $B$  physics will be governed by the soft hadron phenomena, and the uncertainty from the lattice scale is shown by the third error. This uncertainty cancels out in the ratio  $f_{B_s}/f_B$ . We should take these values as provisional until a plateau is actually confirmed with a future dynamical calculation.

### ACKNOWLEDGMENTS

The calculations were performed on the parallel computer CP-PACS at the Center for Computational Physics, University of Tsukuba. This work is supported in part by the Grants-in-Aid of Ministry of Education (Nos. 09304029, 10640246, 10640248, 10740107, 11640250, 11640294, 11740162). TM and AAK are supported by the JSPS Research for the Future Program (Project No. JSPS-RFTF 97P01102). SE, KN and HPS are JSPS Research Fellows.

$\beta = 1.95$ on a $16^3 \times 32$ lattice				
$K_{sea}$	0.1375	0.1390	0.1400	0.1410
# config	648	505	670	397
$K_{val}$	0.1375	0.1375	0.1375	0.1375
	0.1390	0.1390	0.1390	0.1390
	0.1400	0.1400	0.1400	0.1400
	0.1410	0.1410	0.1410	0.1410
	0.1415	0.1415	0.1415	0.1415
$(aM_0, n)$	(2.4,2)	(2.4,2)	(2.4,2)	(2.4,2)
	(2.9,2)	(2.9,2)	(2.9,2)	(2.9,2)
	(3.4,2)	(3.4,2)	(3.4,2)	(3.4,2)
	(4.0,2)	(4.0,2)	(4.0,2)	(4.0,2)
	(4.8,2)	(4.8,2)	(4.8,2)	(4.8,2)
$\beta = 2.1$ on a $24^3 \times 48$ lattice				
$K_{sea}$	0.1357	0.1367	0.1374	0.1382
# config	400	403	379	420
$K_{val}$	0.1357	0.1357	0.1357	0.1357
	0.1364	0.1364	0.1364	0.1364
	0.1374	0.1374	0.1374	0.1374
	0.1382	0.1382	0.1382	0.1382
	0.1385	0.1385	0.1385	0.1385
$(aM_0, n)$	(2.4,2)	(2.4,2)	(2.4,2)	(2.4,2)
	(2.6,2)	(2.6,2)	(2.6,2)	(2.6,2)
	(2.9,2)	(2.9,2)	(2.9,2)	(2.9,2)
	(3.2,2)	(3.2,2)	(3.2,2)	(3.2,2)
	(3.5,2)	(3.5,2)	(3.5,2)	(3.5,2)

TABLE I. Full QCD run parameters.

$\beta$	2.187	2.281	2.334	2.575
lattice	$16^3 \times 32$	$16^3 \times 32$	$16^3 \times 32$	$24^3 \times 48$
# config	195	200	200	200
$K_{val}$	0.1351	0.1343	0.1337	0.1329
	0.1365	0.1357	0.1349	0.1337
	0.1375	0.1367	0.1358	0.1344
	0.1385	0.1377	0.1368	0.1351
	0.1390	0.1383	0.1374	0.1353
$(aM_0, n)$	(2.4,2)	(2.4,2)	(2.4,2)	(2.4,2)
	(2.9,2)	(2.9,2)	(2.9,2)	(2.6,2)
	(3.4,2)	(3.4,2)	(3.4,2)	(2.9,2)
	(4.0,2)	(4.0,2)	(4.0,2)	(3.2,2)
	(4.8,2)	(4.8,2)	(4.8,2)	(3.5,2)

TABLE II. Quenched run parameters.

lattice	Full QCD simulations						Quenched simulations		
	$\beta$	$c_{sw}$	$K_{sea}$	#traj.	$m_\pi/m_\rho$	$a_\sigma$ [fm]	$\beta$	$c_{sw}$	$a_\sigma$ [fm]
$12^3 \times 24$	1.80	1.60	0.1409	6250	0.806(1)	0.289(3)			
			0.1430	5000	0.753(1)	0.280(4)			
			0.1445	7000	0.696(2)	0.269(3)			
			0.1464	5250	0.548(4)	0.248(2)			
$16^3 \times 32$	1.95	1.53	0.1375	7000	0.805(1)	0.204(1)	2.187	1.439	0.2079(15)
			0.1390	7000	0.751(1)	0.193(2)	2.214	1.431	0.1977(13)
			0.1400	7000	0.688(1)	0.181(1)	2.247	1.422	0.1853(9)
			0.1410	7000	0.586(3)	0.170(1)	2.281	1.412	0.1727(10)
$24^3 \times 48$	2.10	1.47	0.1357	4000	0.806(1)	0.1342(6)	2.416	1.379	0.1359(7)
			0.1367	4000	0.755(2)	0.1259(5)	2.456	1.370	0.1266(13)
			0.1374	4000	0.691(3)	0.1201(5)	2.487	1.363	0.1206(9)
			0.1382	4000	0.576(3)	0.1128(3)	2.528	1.355	0.1130(9)
$24^3 \times 48$	2.20	1.44	0.1351	2000	0.800(2)	0.1049(2)			
			0.1358	2000	0.752(3)	0.1012(3)			
			0.1363	2000	0.702(3)	0.0977(3)			
			0.1368	2000	0.637(6)	0.0947(2)			

TABLE III. Overview of full QCD and quenched configurations. The scale  $a_\sigma$ , fixed by assuming  $\sqrt{\sigma} = 440$  MeV, is shown to illustrate the matching of scales (measurement of  $\sigma$  at  $\beta = 2.10$  is made for the first 2000 trajectories). The quenched runs have 200 configurations for each  $\beta$ .

$\beta$	1.95				
$K_{sea}$	0.1375	0.1390	0.1400	0.1410	physical
$\alpha_{\overline{MS}}(1/a)$	0.2241	0.2241	0.2241	0.2241	0.2241
$K_c$	0.144221(10)	0.143648(11)	0.143214(13)	0.142737(11)	0.142065(13)
$a_\rho^{-1}$ [GeV]	0.990(4)	1.048(5)	1.097(6)	1.191(9)	1.269(14)
$K_l$	0.144056(10)	0.143498(11)	0.143073(13)	0.142613(11)	0.141998(12)
$K_s(K)$	0.13998(4)	0.13979(4)	0.13960(4)	0.13956(5)	0.13928(6)
$K_s(\Phi)$	0.13908(6)	0.13896(7)	0.13885(7)	0.13899(8)	0.13863(8)
$a_\Upsilon^{-1}$ [GeV]	1.115(8)	1.185(25)	1.242(12)	1.337(15)	1.469(53)
$K_l$	0.144091(10)	0.143530(11)	0.143104(12)	0.142638(10)	
$K_s(K)$	0.140870(8)	0.140608(9)	0.140373(8)	0.140190(10)	
$K_s(\Phi)$	0.13965(4)	0.13949(4)	0.13935(4)	0.13940(5)	
$\beta$	2.1				
$K_{sea}$	0.1357	0.1367	0.1374	0.1382	physical
$\alpha_{\overline{MS}}(1/a)$	0.204	0.204	0.204	0.204	0.204
$K_c$	0.139748(19)	0.13954(3)	0.139388(13)	0.139238(10)	0.139022(19)
$a_\rho^{-1}$ [GeV]	1.435(15)	1.529(12)	1.579(16)	1.670(24)	1.789(35)
$K_l$	0.139652(19)	0.13945(3)	0.139306(11)	0.139160(10)	0.138967(18)
$K_s(K)$	0.13730(5)	0.13732(4)	0.13727(4)	0.13727(6)	0.13726(7)
$K_s(\Phi)$	0.13686(10)	0.13701(8)	0.13700(7)	0.13701(10)	0.13701(10)
$a_\Upsilon^{-1}$ [GeV]	1.772(25)			2.010(35)	
$K_l$	0.139684(18)			0.139183(9)	
$K_s(K)$	0.138111(10)			0.137835(9)	
$K_s(\Phi)$	0.13740(6)			0.13737(5)	

TABLE IV. Lattice spacings and physical values of the valence hopping parameter  $K$  for full QCD.

$\beta$	2.187	2.281	2.334	2.575
$\alpha_{\overline{MS}}(1/a)$	0.2242	0.2122	0.2062	0.1829
$K_c$	0.141666(12)	0.139587(15)	0.138728(13)	0.136116(8)
$a_\rho^{-1}$ [GeV]	1.017(10)	1.116(12)	1.207(12)	1.743(17)
$K_l$	0.141504(12)	0.139451(14)	0.138604(13)	0.136036(7)
$K_s(K)$	0.13747(8)	0.13609(8)	0.13552(6)	0.13409(4)
$K_s(\Phi)$	0.13651(15)	0.13522(15)	0.13477(11)	0.13368(7)
$a_\Upsilon^{-1}$ [GeV]	1.197(19)	1.397(16)		
$K_l$	0.141557	0.139510		
$K_s(K)$	0.138824	0.137351		
$K_s(\Phi)$	0.137421	0.136161		

TABLE V. Lattice spacings and physical values of the hopping parameter  $K$  for the quenched QCD runs.

$\beta$	$f_B$ (MeV)	$f_{B_s}$ (MeV)		$f_{B_s}/f_B$	
		$K$ input	$\Phi$ input	$K$ input	$\Phi$ input
scale from $m_\rho$					
2.187	224(6)	256(5)	265(5)	1.146(10)	1.184(12)
2.281	199(7)	230(6)	239(6)	1.154(20)	1.197(25)
2.334	185(6)	217(5)	226(5)	1.177(18)	1.222(23)
2.575	191(4)	220(4)	226(5)	1.150(9)	1.184(12)
scale from $\Upsilon$					
2.187	269(8)	295(8)	309(8)	1.094(6)	1.149(9)
2.281	257(9)	282(8)	297(7)	1.096(11)	1.154(18)

TABLE VI. Quenched decay constants.

$K_{sea}$	$f_B$ (MeV)	$f_{B_s}$ (MeV)		$f_{B_s}/f_B$	
		$K$ input	$\Phi$ input	$K$ input	$\Phi$ input
scale from $m_\rho$					
$\beta = 1.95$					
0.1375	230(4)	266(4)	275(4)	1.156(9)	1.194(11)
0.1390	233(7)	266(6)	275(6)	1.144(14)	1.179(17)
0.1400	220(5)	259(4)	268(4)	1.174(10)	1.215(13)
0.1410	228(6)	266(5)	273(6)	1.167(15)	1.200(18)
$\beta = 2.1$					
0.1357	193(5)	225(5)	232(5)	1.166(12)	1.199(14)
0.1367	206(6)	238(5)	243(6)	1.159(11)	1.184(13)
0.1374	197(5)	231(6)	235(6)	1.172(11)	1.196(12)
0.1382	201(8)	236(9)	242(8)	1.177(15)	1.203(17)
scale from $\Upsilon$					
$\beta = 1.95$					
0.1375	264(5)	295(4)	309(4)	1.118(7)	1.168(10)
0.1390	266(10)	294(10)	306(10)	1.108(9)	1.154(13)
0.1400	254(7)	286(6)	300(6)	1.130(7)	1.183(10)
0.1410	259(8)	293(7)	305(7)	1.130(12)	1.176(15)
$\beta = 2.1$					
0.1357	250(7)	276(7)	289(7)	1.104(9)	1.155(13)
0.1382	249(11)	279(11)	290(11)	1.118(11)	1.162(14)

TABLE VII. Partially quenched decay constants.

$\beta$	$f_B$ (MeV)	$f_{B_s}$ (MeV)		$f_{B_s}/f_B$	
		$K$ input	$\Phi$ input	$K$ input	$\Phi$ input
		scale from $m_\rho$			
1.95	222(6)	261(5)	268(6)	1.176(14)	1.212(17)
2.1	204(8)	242(9)	245(9)	1.179(18)	1.198(20)
		scale from $\Upsilon$			
1.95	254(8)	287(7)	300(7)	1.134(10)	1.183(14)
2.1	249(16)	280(16)	290(16)	1.124(16)	1.165(21)

TABLE VIII. Decay constants in full QCD.

$\beta$	$N_f = 0$ lattices				$N_f = 2$ lattices	
	2.187	2.281	2.334	2.575	1.95	2.1
$O(a^2\Lambda_{QCD}^2)$	35 %	29 %	25 %	12 %	22 %	11 %
$O(\alpha_s a\Lambda_{QCD})$	13 %	11 %	10 %	6 %	11 %	7 %
$O(\alpha_s^2)$	5 %	5 %	4 %	3 %	5 %	4 %
$O(\alpha_s\Lambda_{QCD}/M_b)$	3 %	3 %	3 %	2 %	3 %	3 %
$O(\alpha_s^2/(aM_b))$	1 %	1 %	1 %	1 %	1 %	2 %
$O(\Lambda_{QCD}^2/M_b^2)$	2 %	2 %	2 %	1 %	2 %	2 %
$O(\Lambda_{QCD}^2 a/M_b)$	8 %	7 %	7 %	4 %	6 %	4 %
total error for $f_B$ and $f_{B_s}$	39 %	32 %	28 %	14 %	26 %	14 %
total error for $f_{B_s}/f_B - 1$	37 %	31 %	27 %	13 %	25 %	13 %

TABLE IX. Estimated systematic errors.  $\alpha_{\overline{MS}}(1/a)$  and  $\Lambda_{QCD} = 600$  MeV are used.

APPENDIX

$\beta = 1.95$					
$aM_0$	$K_{val} = 0.1375$	$K_{val} = 0.1390$	$K_{val} = 0.1400$	$K_{val} = 0.1410$	$K_{val} = 0.1415$
$K_{sea} = 0.1375$					
2.4	3.45(4)	3.38(4)	3.34(5)	3.31(6)	3.29(6)
2.9	3.95(5)	3.88(5)	3.83(6)	3.80(7)	3.79(8)
3.4	4.43(6)	4.36(7)	4.31(8)	4.28(9)	4.28(10)
4.0	5.01(7)	4.93(9)	4.88(10)	4.85(12)	4.85(14)
4.8	5.76(10)	5.67(12)	5.62(13)	5.60(16)	5.61(19)
$K_{sea} = 0.1390$					
2.4	3.41(6)	3.36(7)	3.34(9)	3.36(13)	3.42(16)
2.9	3.91(8)	3.86(10)	3.85(12)	3.90(17)	3.99(23)
3.4	4.41(10)	4.36(13)	4.35(16)	4.43(24)	4.56(32)
4.0	4.99(13)	4.94(17)	4.94(22)	5.07(33)	5.27(45)
4.8	5.75(19)	5.69(25)	5.72(32)	5.92(49)	6.25(69)
$K_{sea} = 0.1400$					
2.4	3.39(5)	3.31(8)	3.28(11)	3.28(11)	3.28(14)
2.9	3.92(7)	3.83(11)	3.82(15)	3.82(15)	3.82(20)
3.4	4.44(9)	4.36(15)	4.35(21)	4.35(21)	4.38(27)
4.0	5.06(13)	4.99(21)	5.01(30)	5.01(30)	5.07(39)
4.8	6.01(21)	5.81(32)	5.89(46)	5.89(46)	6.03(62)
$K_{sea} = 0.1410$					
2.4	3.22(6)	3.13(7)	3.06(9)	2.98(11)	2.99(19)
2.6	3.68(8)	3.58(9)	3.50(11)	3.51(19)	3.48(24)
2.9	4.12(9)	4.00(11)	3.91(14)	3.99(24)	3.98(30)
3.2	4.63(12)	4.49(14)	4.39(17)	4.56(31)	4.59(40)
3.5	5.27(15)	5.11(19)	4.99(23)	5.33(45)	5.42(59)
$\beta = 2.1$					
$aM_0$	$K_{val} = 0.1357$	$K_{val} = 0.1367$	$K_{val} = 0.1374$	$K_{val} = 0.1382$	$K_{val} = 0.1385$
$K_{sea} = 0.1357$					
2.4	3.37(9)	3.26(14)	3.29(18)	3.39(27)	3.34(34)
2.6	3.44(13)	3.48(17)	3.51(21)	3.63(33)	3.58(41)
2.9	3.74(17)	3.80(21)	3.89(27)	4.00(43)	3.93(54)
3.2	4.04(21)	4.13(26)	4.19(34)	4.38(56)	4.28(71)
3.5	4.34(25)	4.45(33)	4.53(42)	4.78(72)	4.66(48)
$K_{sea} = 0.1367$					
2.4	3.04(9)	3.03(10)	3.04(11)	3.03(14)	3.04(16)
2.6	3.23(10)	3.23(11)	3.24(13)	3.22(16)	3.24(18)
2.9	3.51(12)	3.52(14)	3.53(16)	3.52(20)	3.54(23)
3.2	3.79(14)	3.81(17)	3.83(19)	3.81(25)	3.84(27)
3.5	4.07(17)	4.09(10)	4.13(23)	4.10(30)	4.13(33)
$K_{sea} = 0.1374$					
2.4	3.13(9)	3.09(11)	3.05(12)	3.00(15)	2.96(18)
2.6	3.33(11)	3.28(12)	3.24(13)	3.19(17)	3.14(20)
2.9	3.62(12)	3.56(14)	3.52(15)	3.46(21)	3.42(24)
3.2	3.91(14)	3.84(16)	3.79(18)	3.74(24)	3.70(29)
3.5	4.19(16)	4.11(18)	4.05(20)	4.01(28)	3.98(34)
$K_{sea} = 0.1382$					
2.4	2.95(8)	2.93(10)	2.93(13)	2.92(18)	2.94(22)
2.6	3.12(8)	3.11(11)	3.11(14)	3.12(20)	3.13(25)
2.9	3.39(10)	3.38(13)	3.39(16)	3.40(24)	3.42(29)
3.2	3.65(11)	3.65(15)	3.67(19)	3.68(28)	3.69(34)
3.5	3.91(11)	3.92(17)	3.94(22)	3.95(32)	3.96(40)

TABLE X. Kinetic masses in lattice units measured from the dispersion relation in full QCD.

$\beta = 2.187$					
$aM_0$	$K = 0.1351$	$K = 0.1365$	$K = 0.1375$	$K = 0.1385$	$K = 0.1390$
2.4	3.36(8)	3.29(8)	3.26(9)	3.23(11)	3.24(12)
2.9	3.84(9)	3.79(10)	3.76(12)	3.73(14)	3.71(15)
3.4	4.33(11)	4.28(13)	4.25(15)	4.22(17)	4.21(19)
4.0	4.91(14)	4.86(17)	4.83(19)	4.82(23)	4.82(25)
4.8	5.65(19)	5.61(23)	5.60(27)	5.62(32)	5.65(35)
$\beta = 2.281$					
$aM_0$	$K = 0.1343$	$K = 0.1357$	$K = 0.1367$	$K = 0.1377$	$K = 0.1383$
2.4	3.35(7)	3.28(8)	3.22(9)	3.17(11)	3.17(14)
2.9	3.88(9)	3.79(11)	3.72(12)	3.66(15)	3.64(18)
3.4	4.40(12)	4.29(14)	4.20(16)	4.13(19)	4.10(23)
4.0	5.01(16)	4.88(18)	4.78(21)	4.67(25)	4.63(30)
4.8	5.82(23)	5.66(26)	5.51(29)	5.38(35)	5.32(41)
$\beta = 2.334$					
$aM_0$	$K = 0.1337$	$K = 0.1349$	$K = 0.1358$	$K = 0.1368$	$K = 0.1374$
2.4	3.17(7)	3.11(7)	3.08(8)	3.04(9)	3.03(11)
2.9	3.64(9)	3.58(10)	3.54(11)	3.51(12)	3.47(15)
3.4	4.10(11)	4.04(12)	4.00(14)	3.96(16)	3.90(19)
4.0	4.64(15)	4.57(16)	4.52(18)	4.41(20)	4.39(24)
4.8	5.33(20)	5.25(22)	5.19(24)	5.03(27)	5.00(32)
$\beta = 2.575$					
$aM_0$	$K = 0.1329$	$K = 0.1337$	$K = 0.1344$	$K = 0.1351$	$K = 0.1353$
2.4	2.77(09)	2.71(11)	2.65(13)	2.57(17)	2.55(19)
2.6	2.94(10)	2.87(12)	2.89(15)	2.73(19)	2.69(22)
2.9	3.18(12)	3.11(14)	3.04(18)	2.95(23)	2.91(26)
3.2	3.43(14)	3.35(17)	3.26(21)	3.17(28)	3.13(31)
3.5	3.67(16)	3.58(20)	3.49(24)	3.38(33)	3.34(36)

TABLE XI. Kinetic masses in lattice units measured from the dispersion relation in the quenched case.



$\beta = 1.95$					
$aM^0$	$K_{val} = 0.1375$	$K_{val} = 0.1390$	$K_{val} = 0.1400$	$K_{val} = 0.1410$	$K_{val} = 0.1415$
$K_{sea} = 0.1375$					
2.4	0.712(1)	0.679(1)	0.657(2)	0.635(2)	0.624(2)
2.9	0.730(1)	0.697(1)	0.675(2)	0.654(2)	0.643(2)
3.4	0.741(1)	0.709(2)	0.688(2)	0.667(2)	0.656(2)
4.0	0.750(1)	0.719(2)	0.698(2)	0.677(2)	0.667(2)
4.8	0.757(2)	0.727(2)	0.706(2)	0.686(2)	0.676(3)
$K_{sea} = 0.1390$					
2.4	0.694(2)	0.661(2)	0.639(2)	0.617(2)	0.607(3)
2.9	0.712(2)	0.679(2)	0.658(2)	0.637(3)	0.627(3)
3.4	0.724(2)	0.692(2)	0.671(2)	0.650(3)	0.640(3)
4.0	0.734(2)	0.703(2)	0.682(2)	0.662(3)	0.652(3)
4.8	0.743(2)	0.712(2)	0.692(3)	0.672(3)	0.662(4)
$K_{sea} = 0.1400$					
2.4	0.677(1)	0.641(2)	0.618(2)	0.594(2)	0.582(3)
2.9	0.694(2)	0.659(2)	0.636(2)	0.613(3)	0.601(3)
3.4	0.705(2)	0.671(2)	0.649(2)	0.626(3)	0.614(3)
4.0	0.715(2)	0.681(2)	0.659(2)	0.636(3)	0.624(3)
4.8	0.723(2)	0.690(2)	0.667(3)	0.645(3)	0.634(4)
$K_{sea} = 0.1410$					
2.4	0.656(2)	0.620(2)	0.596(3)	0.573(3)	0.561(3)
2.9	0.673(2)	0.637(2)	0.614(3)	0.591(3)	0.580(4)
3.4	0.684(2)	0.649(2)	0.627(3)	0.604(3)	0.592(4)
4.0	0.693(2)	0.659(3)	0.637(3)	0.614(4)	0.603(4)
4.8	0.701(2)	0.668(3)	0.646(3)	0.624(4)	0.612(4)
$\beta = 2.1$					
$aM^0$	$K_{val} = 0.1357$	$K_{val} = 0.1367$	$K_{val} = 0.1374$	$K_{val} = 0.1382$	$K_{val} = 0.1385$
$K_{sea} = 0.1357$					
2.4	0.585(2)	0.559(2)	0.540(2)	0.519(3)	0.510(3)
2.6	0.592(2)	0.566(2)	0.547(2)	0.526(3)	0.517(3)
2.9	0.600(2)	0.574(2)	0.555(2)	0.534(3)	0.526(3)
3.2	0.606(2)	0.580(2)	0.562(2)	0.541(3)	0.532(3)
3.5	0.611(2)	0.585(2)	0.567(2)	0.546(3)	0.538(3)
$K_{sea} = 0.1367$					
2.4	0.575(2)	0.548(2)	0.529(2)	0.507(3)	0.499(3)
2.6	0.582(2)	0.555(2)	0.536(2)	0.514(3)	0.506(3)
2.9	0.590(2)	0.563(2)	0.544(2)	0.523(3)	0.515(3)
3.2	0.596(2)	0.570(2)	0.551(2)	0.530(3)	0.522(3)
3.5	0.601(2)	0.575(2)	0.556(3)	0.536(3)	0.528(4)
$K_{sea} = 0.1374$					
2.4	0.564(2)	0.536(2)	0.516(2)	0.494(3)	0.485(3)
2.6	0.570(2)	0.542(2)	0.523(2)	0.500(3)	0.492(3)
2.9	0.578(2)	0.550(2)	0.531(2)	0.509(3)	0.500(3)
3.2	0.584(2)	0.557(2)	0.538(2)	0.515(3)	0.507(3)
3.5	0.589(2)	0.562(2)	0.543(2)	0.521(3)	0.512(3)
$K_{sea} = 0.1382$					
2.4	0.553(2)	0.524(2)	0.505(3)	0.483(3)	0.476(4)
2.6	0.559(2)	0.531(2)	0.511(3)	0.490(3)	0.483(4)
2.9	0.567(2)	0.539(3)	0.519(3)	0.498(3)	0.491(4)
3.2	0.574(2)	0.546(3)	0.526(3)	0.505(3)	0.498(4)
3.5	0.579(2)	0.551(3)	0.532(3)	0.510(4)	0.503(4)

TABLE XII. Simulation energies in full QCD, in lattice units.

$\beta = 2.187$					
$aM_0$	$K = 0.1351$	$K = 0.1365$	$K = 0.1375$	$K = 0.1385$	$K = 0.1390$
2.4	0.707(2)	0.675(2)	0.652(3)	0.629(3)	0.617(3)
2.6	0.724(2)	0.693(2)	0.671(3)	0.649(3)	0.637(4)
2.9	0.736(2)	0.706(2)	0.684(3)	0.662(3)	0.651(4)
3.2	0.746(2)	0.716(3)	0.694(3)	0.673(3)	0.662(4)
3.5	0.754(2)	0.725(3)	0.704(3)	0.683(3)	0.672(4)
$\beta = 2.281$					
$aM_0$	$K = 0.1343$	$K = 0.1357$	$K = 0.1367$	$K = 0.1377$	$K = 0.1383$
2.4	0.648(2)	0.614(3)	0.590(3)	0.566(4)	0.551(4)
2.9	0.664(3)	0.631(3)	0.608(3)	0.584(4)	0.569(5)
3.4	0.674(3)	0.642(3)	0.619(4)	0.597(5)	0.582(5)
4.0	0.683(3)	0.652(3)	0.629(4)	0.607(5)	0.593(5)
4.8	0.691(3)	0.660(3)	0.639(4)	0.617(5)	0.604(5)
$\beta = 2.334$					
$aM_0$	$K = 0.1337$	$K = 0.1349$	$K = 0.1358$	$K = 0.1368$	$K = 0.1374$
2.4	0.623(2)	0.592(3)	0.569(3)	0.544(4)	0.529(5)
2.9	0.638(2)	0.608(3)	0.586(3)	0.561(4)	0.546(5)
3.4	0.648(2)	0.619(3)	0.597(3)	0.572(4)	0.558(5)
4.0	0.657(3)	0.628(3)	0.606(3)	0.582(4)	0.568(5)
4.8	0.665(3)	0.636(3)	0.615(4)	0.591(5)	0.577(6)
$\beta = 2.575$					
$aM_0$	$K = 0.1329$	$K = 0.1337$	$K = 0.1344$	$K = 0.1351$	$K = 0.1353$
2.4	0.501(2)	0.478(2)	0.459(2)	0.440(3)	0.435(3)
2.9	0.506(2)	0.484(2)	0.464(3)	0.446(3)	0.441(3)
3.4	0.513(2)	0.491(2)	0.472(3)	0.454(3)	0.449(4)
4.0	0.518(2)	0.496(2)	0.478(3)	0.460(3)	0.455(4)
4.8	0.523(2)	0.501(2)	0.482(3)	0.465(3)	0.460(4)

TABLE XIII. Quenched simulation energies, in lattice units.

$\beta = 1.95$					
$aM_0$	$K_{val} = 0.1375$	$K_{val} = 0.1390$	$K_{val} = 0.1400$	$K_{val} = 0.1410$	$K_{val} = 0.1415$
$K_{sea} = 0.1375$					
2.4	3.08(15)	3.04(15)	3.02(15)	3.00(15)	2.99(15)
2.9	3.64(18)	3.60(18)	3.58(18)	3.56(18)	3.55(18)
3.4	4.18(21)	4.15(21)	4.13(21)	4.11(21)	4.10(21)
4.0	4.83(24)	4.80(24)	4.78(24)	4.76(24)	4.75(24)
4.8	5.69(28)	5.66(28)	5.64(28)	5.62(28)	5.61(28)
$K_{sea} = 0.1390$					
2.4	3.06(15)	3.02(15)	3.00(15)	2.98(15)	2.97(15)
2.9	3.62(18)	3.59(18)	3.56(18)	3.54(18)	3.53(18)
3.4	4.17(21)	4.14(21)	4.11(21)	4.09(20)	4.08(20)
4.0	4.82(24)	4.79(24)	4.76(24)	4.74(24)	4.73(24)
4.8	5.67(28)	5.64(28)	5.62(28)	5.60(28)	5.59(28)
$K_{sea} = 0.1400$					
2.4	3.04(15)	3.00(15)	2.98(15)	2.96(15)	2.95(15)
2.9	3.60(18)	3.57(18)	3.54(18)	3.52(18)	3.51(18)
3.4	4.15(21)	4.12(21)	4.09(20)	4.07(20)	4.06(20)
4.0	4.80(24)	4.76(24)	4.74(24)	4.72(24)	4.71(24)
4.8	5.65(28)	5.62(28)	5.60(28)	5.57(28)	5.56(28)
$K_{sea} = 0.1410$					
2.4	3.02(15)	2.98(15)	2.96(15)	2.94(15)	2.92(15)
2.6	3.58(18)	3.54(18)	3.52(18)	3.50(18)	3.49(17)
2.9	4.13(21)	4.09(20)	4.07(20)	4.05(20)	4.04(20)
3.2	4.78(24)	4.74(24)	4.72(24)	4.70(24)	4.69(23)
3.5	5.63(28)	5.60(28)	5.58(28)	5.55(28)	5.54(28)
$\beta = 2.1$					
$aM_0$	$K_{val} = 0.1357$	$K_{val} = 0.1367$	$K_{val} = 0.1374$	$K_{val} = 0.1382$	$K_{val} = 0.1385$
$K_{sea} = 0.1357$					
2.4	2.95(12)	2.93(12)	2.91(12)	2.89(12)	2.88(12)
2.6	3.18(13)	3.15(13)	3.13(13)	3.11(12)	3.10(12)
2.9	3.51(14)	3.48(14)	3.46(14)	3.44(14)	3.43(14)
3.2	3.83(15)	3.81(15)	3.79(15)	3.77(15)	3.76(15)
3.5	4.16(17)	4.13(17)	4.11(16)	4.09(16)	4.08(16)
$K_{sea} = 0.1367$					
2.4	2.94(12)	2.91(12)	2.90(12)	2.87(12)	2.87(12)
2.6	3.17(13)	3.14(13)	3.12(12)	3.10(12)	3.09(12)
2.9	3.50(14)	3.47(14)	3.45(14)	3.43(14)	3.42(14)
3.2	3.82(15)	3.80(15)	3.78(15)	3.76(15)	3.75(15)
3.5	4.15(17)	4.12(16)	4.10(16)	4.08(16)	4.07(16)
$K_{sea} = 0.1374$					
2.4	2.93(12)	2.90(12)	2.88(12)	2.86(11)	2.85(11)
2.6	3.15(13)	3.13(13)	3.11(12)	3.08(12)	3.08(12)
2.9	3.48(14)	3.46(14)	3.44(14)	3.41(14)	3.41(14)
3.2	3.81(15)	3.78(15)	3.76(15)	3.74(15)	3.73(15)
3.5	4.14(17)	4.11(16)	4.09(16)	4.07(16)	4.06(16)
$K_{sea} = 0.1382$					
2.4	2.92(12)	2.89(12)	2.87(11)	2.85(11)	2.84(11)
2.6	3.14(13)	3.11(12)	3.09(12)	3.07(12)	3.07(12)
2.9	3.47(14)	3.44(14)	3.43(14)	3.40(14)	3.40(14)
3.2	3.80(15)	3.77(15)	3.75(15)	3.73(15)	3.72(15)
3.5	4.13(17)	4.10(16)	4.08(16)	4.06(16)	4.05(16)

TABLE XIV. Meson masses with the perturbative mass shifts in full QCD, in lattice units.

$\beta = 2.187$					
$aM_0$	$K = 0.1351$	$K = 0.1365$	$K = 0.1375$	$K = 0.1385$	$K = 0.1390$
2.4	3.07(15)	3.04(15)	3.02(15)	2.99(15)	2.98(15)
2.9	3.63(18)	3.60(18)	3.58(18)	3.55(18)	3.54(18)
3.4	4.18(21)	4.15(21)	4.13(21)	4.11(21)	4.09(20)
4.0	4.83(24)	4.80(24)	4.78(24)	4.76(24)	4.75(24)
4.8	5.68(28)	5.65(28)	5.63(28)	5.61(28)	5.60(28)
$\beta = 2.281$					
$aM_0$	$K = 0.1343$	$K = 0.1357$	$K = 0.1367$	$K = 0.1377$	$K = 0.1383$
2.4	3.01(15)	2.98(15)	2.96(15)	2.93(15)	2.92(15)
2.9	3.57(18)	3.54(18)	3.51(18)	3.49(17)	3.48(17)
3.4	4.12(21)	4.08(20)	4.06(20)	4.04(20)	4.02(20)
4.0	4.76(24)	4.73(24)	4.71(24)	4.69(23)	4.67(23)
4.8	5.61(28)	5.58(28)	5.56(28)	5.54(28)	5.53(28)
$\beta = 2.334$					
$aM_0$	$K = 0.1337$	$K = 0.1349$	$K = 0.1358$	$K = 0.1368$	$K = 0.1374$
2.4	2.99(12)	2.96(12)	2.94(12)	2.91(12)	2.90(12)
2.9	3.54(14)	3.51(14)	3.49(14)	3.47(14)	3.45(14)
3.4	4.09(16)	4.06(16)	4.04(16)	4.01(16)	4.00(16)
4.0	4.73(19)	4.70(19)	4.68(19)	4.66(19)	4.64(19)
4.8	5.58(22)	5.56(22)	5.53(22)	5.51(22)	5.50(22)
$\beta = 2.575$					
$aM_0$	$K = 0.1329$	$K = 0.1337$	$K = 0.1344$	$K = 0.1351$	$K = 0.1353$
2.4	2.87(9)	2.85(9)	2.83(8)	2.81(8)	2.81(8)
2.6	3.09(9)	3.07(9)	3.05(9)	3.03(9)	3.03(9)
2.9	3.42(10)	3.40(10)	3.38(10)	3.36(10)	3.36(10)
3.2	3.75(11)	3.72(11)	3.70(11)	3.69(11)	3.68(12)
3.5	4.07(12)	4.05(12)	4.03(12)	4.01(12)	4.00(12)

TABLE XV. Quenched meson masses with perturbative mass shifts, in lattice units.

$\beta$	$K_{sea}$	scale from $\rho$	scale from $\Upsilon$
1.95	0.1375	4.53(12)	4.43(13)
	0.1390	4.29(26)	4.14(28)
	0.1400	4.26(21)	4.18(23)
	0.1410	4.88(23)	4.77(23)
2.1	0.1357	4.08(34)	3.95(30)
	0.1367	4.45(24)	
	0.1374	4.41(25)	
	0.1382	4.65(42)	4.44(43)

TABLE XVI. Bare  $b$  quark masses  $M_{0b}$ , in GeV, for the full QCD lattices. Results with two different scale determinations,  $m_\rho$  and  $\Upsilon$  are listed for each sea quark mass.

$\beta$	scale from $\rho$	scale from $\Upsilon$
2.187	4.55(24)	4.42(25)
2.281	4.45(23)	4.32(24)
2.334	4.54(27)	
2.575	5.15(39)	

TABLE XVII. Bare  $b$  quark masses  $M_{0b}$ , in GeV, for the quenched lattices. Results with two different scale determinations,  $m_\rho$  and  $\Upsilon$  are listed for each sea quark mass.

$a^{3/2}(f\sqrt{M})^{(0)}$					
$aM_0$	$K_{val} = 0.1375$	$K_{val} = 0.1390$	$K_{val} = 0.1400$	$K_{val} = 0.1410$	$K_{val} = 0.1415$
$K_{sea} = 0.1375$					
2.4	0.567(5)	0.576(5)	0.595(4)	0.613(4)	0.640(4)
2.9	0.595(6)	0.606(5)	0.626(5)	0.646(4)	0.676(4)
3.4	0.619(6)	0.630(6)	0.652(5)	0.674(5)	0.705(5)
4.0	0.643(7)	0.655(6)	0.678(6)	0.702(5)	0.736(5)
4.8	0.669(7)	0.682(7)	0.707(6)	0.732(6)	0.768(6)
$K_{sea} = 0.1390$					
2.4	0.534(7)	0.543(6)	0.561(5)	0.579(5)	0.606(5)
2.9	0.561(7)	0.571(7)	0.591(6)	0.611(6)	0.640(5)
3.4	0.586(10)	0.597(9)	0.619(8)	0.641(7)	0.673(7)
4.0	0.612(11)	0.623(10)	0.646(9)	0.670(8)	0.704(7)
4.8	0.641(13)	0.653(11)	0.678(10)	0.702(09)	0.739(8)
$K_{sea} = 0.1400$					
2.4	0.484(6)	0.496(5)	0.518(4)	0.539(4)	0.570(4)
2.9	0.508(6)	0.520(6)	0.544(5)	0.567(5)	0.600(4)
3.4	0.527(7)	0.540(6)	0.566(5)	0.590(5)	0.626(5)
4.0	0.546(8)	0.560(7)	0.588(6)	0.614(5)	0.652(5)
4.8	0.567(9)	0.582(8)	0.612(7)	0.640(6)	0.680(6)
$K_{sea} = 0.1410$					
2.4	0.429(7)	0.441(6)	0.462(5)	0.484(5)	0.514(5)
2.9	0.449(9)	0.462(7)	0.486(6)	0.509(6)	0.542(5)
3.4	0.465(9)	0.479(8)	0.505(7)	0.530(6)	0.565(6)
4.0	0.482(11)	0.497(9)	0.525(8)	0.551(7)	0.587(6)
4.8	0.501(12)	0.517(10)	0.546(8)	0.573(8)	0.612(7)
$a^{3/2}(f\sqrt{M})^{(1)}$					
$aM_0$	$K_{val} = 0.1375$	$K_{val} = 0.1390$	$K_{val} = 0.1400$	$K_{val} = 0.1410$	$K_{val} = 0.1415$
$K_{sea} = 0.1375$					
2.4	-0.0817(12)	-0.0823(12)	-0.0836(10)	-0.0850(10)	-0.0869(9)
2.9	-0.0730(12)	-0.0735(11)	-0.0748(10)	-0.0761(9)	-0.0779(8)
3.4	-0.0661(11)	-0.0666(11)	-0.0677(9)	-0.0689(9)	-0.0706(8)
4.0	-0.0594(11)	-0.0599(10)	-0.0609(9)	-0.0620(8)	-0.0636(7)
4.8	-0.0524(10)	-0.0528(9)	-0.0538(8)	-0.0547(8)	-0.0562(7)
$K_{sea} = 0.1390$					
2.4	-0.0754(11)	-0.0761(10)	-0.0775(9)	-0.0789(8)	-0.0810(8)
2.9	-0.0672(10)	-0.0678(9)	-0.0691(8)	-0.0705(8)	-0.0724(7)
3.4	-0.0614(11)	-0.0619(10)	-0.0631(9)	-0.0643(8)	-0.0662(7)
4.0	-0.0552(11)	-0.0557(10)	-0.0568(9)	-0.0580(8)	-0.0597(7)
4.8	-0.0488(11)	-0.0493(10)	-0.0503(9)	-0.0514(8)	-0.0530(7)
$K_{sea} = 0.1400$					
2.4	-0.0681(8)	-0.0692(8)	-0.0712(7)	-0.0730(6)	-0.0755(6)
2.9	-0.0604(8)	-0.0614(7)	-0.0633(6)	-0.0650(6)	-0.0674(5)
3.4	-0.0544(8)	-0.0553(7)	-0.0570(6)	-0.0587(5)	-0.0609(5)
4.0	-0.0486(8)	-0.0494(7)	-0.0510(6)	-0.0525(5)	-0.0546(5)
4.8	-0.0425(7)	-0.0433(6)	-0.0447(5)	-0.0461(5)	-0.0481(5)
$K_{sea} = 0.1410$					
2.4	-0.0607(12)	-0.0616(10)	-0.0637(8)	-0.0656(8)	-0.0682(7)
2.9	-0.0537(12)	-0.0545(10)	-0.0565(8)	-0.0583(7)	-0.0607(7)
3.4	-0.0482(11)	-0.0490(9)	-0.0508(8)	-0.0525(7)	-0.0547(6)
4.0	-0.0430(10)	-0.0437(9)	-0.0453(7)	-0.0469(7)	-0.0490(6)
4.8	-0.0376(10)	-0.0382(8)	-0.0397(7)	-0.0411(6)	-0.0430(6)

TABLE XVIII. Decay matrix elements at  $\beta = 1.95$ .

$a^{3/2}(f\sqrt{M})^{(0)}$					
$aM_0$	$K_{val} = 0.1357$	$K_{val} = 0.1367$	$K_{val} = 0.1374$	$K_{val} = 0.1382$	$K_{val} = 0.1385$
$K_{sea} = 0.1357$					
2.4	0.317(5)	0.324(4)	0.341(4)	0.355(4)	0.376(4)
2.6	0.322(5)	0.329(4)	0.346(4)	0.361(4)	0.383(4)
2.9	0.328(5)	0.336(4)	0.354(4)	0.369(4)	0.392(4)
3.2	0.334(5)	0.342(4)	0.360(4)	0.376(4)	0.399(4)
3.5	0.339(5)	0.347(4)	0.366(4)	0.382(4)	0.406(4)
$K_{sea} = 0.1367$					
2.4	0.299(5)	0.306(5)	0.324(4)	0.339(4)	0.360(3)
2.6	0.304(5)	0.311(5)	0.329(4)	0.345(4)	0.366(4)
2.9	0.311(5)	0.318(5)	0.337(4)	0.353(4)	0.375(4)
3.2	0.317(6)	0.324(5)	0.343(4)	0.359(4)	0.382(4)
3.5	0.322(6)	0.329(5)	0.348(5)	0.365(4)	0.389(4)
$K_{sea} = 0.1374$					
2.4	0.275(4)	0.282(4)	0.300(3)	0.316(3)	0.337(4)
2.6	0.278(4)	0.286(4)	0.305(4)	0.321(4)	0.342(4)
2.9	0.284(4)	0.291(4)	0.311(4)	0.327(4)	0.350(4)
3.2	0.288(5)	0.296(4)	0.316(4)	0.333(4)	0.356(4)
3.5	0.292(5)	0.300(5)	0.321(4)	0.338(4)	0.362(4)
$K_{sea} = 0.1382$					
2.4	0.256(5)	0.262(5)	0.281(4)	0.298(4)	0.320(4)
2.6	0.260(6)	0.266(5)	0.285(5)	0.302(4)	0.325(4)
2.9	0.265(6)	0.271(5)	0.291(5)	0.309(5)	0.332(4)
3.2	0.269(6)	0.276(6)	0.296(5)	0.315(5)	0.339(5)
3.5	0.272(7)	0.280(6)	0.301(5)	0.320(5)	0.345(5)
$a^{3/2}(f\sqrt{M})^{(1)}$					
$aM_0$	$K_{val} = 0.1357$	$K_{val} = 0.1367$	$K_{val} = 0.1374$	$K_{val} = 0.1382$	$K_{val} = 0.1385$
$K_{sea} = 0.1357$					
2.4	-0.0381(6)	-0.0387(6)	-0.0403(5)	-0.0416(5)	-0.0435(4)
2.6	-0.0361(6)	-0.0367(5)	-0.0382(5)	-0.0395(5)	-0.0413(4)
2.9	-0.0335(6)	-0.0341(5)	-0.0355(5)	-0.0367(4)	-0.0385(4)
3.2	-0.0312(5)	-0.0318(5)	-0.0332(4)	-0.0343(4)	-0.0360(4)
3.5	-0.0293(5)	-0.0298(4)	-0.0312(4)	-0.0322(4)	-0.0338(4)
$K_{sea} = 0.1367$					
2.4	-0.0356(7)	-0.0363(6)	-0.0379(5)	-0.0393(5)	-0.0412(4)
2.6	-0.0338(6)	-0.0344(6)	-0.0360(5)	-0.0373(5)	-0.0392(4)
2.9	-0.0314(6)	-0.0319(6)	-0.0334(5)	-0.0347(5)	-0.0364(4)
3.2	-0.0292(6)	-0.0298(5)	-0.0312(5)	-0.0324(4)	-0.0341(4)
3.5	-0.0274(5)	-0.0279(5)	-0.0293(5)	-0.0304(4)	-0.0320(4)
$K_{sea} = 0.1374$					
2.4	-0.0322(5)	-0.0329(5)	-0.0346(4)	-0.0361(4)	-0.0381(4)
2.6	-0.0305(5)	-0.0311(5)	-0.0328(4)	-0.0342(4)	-0.0361(4)
2.9	-0.0283(5)	-0.0288(4)	-0.0304(4)	-0.0318(4)	-0.0336(4)
3.2	-0.0263(5)	-0.0268(4)	-0.0283(4)	-0.0296(4)	-0.0313(4)
3.5	-0.0246(4)	-0.0251(4)	-0.0265(4)	-0.0277(3)	-0.0294(3)
$K_{sea} = 0.1382$					
2.4	-0.0300(8)	-0.0306(7)	-0.0322(6)	-0.0337(5)	-0.0359(5)
2.6	-0.0284(7)	-0.0289(6)	-0.0305(5)	-0.0320(5)	-0.0341(5)
2.9	-0.0263(7)	-0.0268(6)	-0.0283(5)	-0.0297(5)	-0.0317(5)
3.2	-0.0245(7)	-0.0250(6)	-0.0264(5)	-0.0278(5)	-0.0296(5)
3.5	-0.0229(6)	-0.0234(6)	-0.0247(5)	-0.0261(5)	-0.0278(5)

TABLE XIX. Decay matrix elements at  $\beta = 2.1$ .

	$K=0.1351$	$K=0.1365$	$K=0.1375$	$K=0.1385$	$K=0.1390$
$aM_0$			$a^{3/2}(f\sqrt{M})^{(0)}$		
2.4	0.539(6)	0.548(6)	0.566(5)	0.583(5)	0.607(5)
2.9	0.566(7)	0.575(6)	0.594(6)	0.613(6)	0.639(5)
3.4	0.588(7)	0.598(7)	0.618(6)	0.638(6)	0.665(5)
4.0	0.610(7)	0.621(7)	0.642(7)	0.663(6)	0.692(6)
4.8	0.634(8)	0.646(7)	0.668(7)	0.690(7)	0.721(6)
$aM_0$			$a^{3/2}(f\sqrt{M})^{(1)}$		
2.4	-0.0744(11)	-0.0748(10)	-0.0761(9)	-0.0772(9)	-0.0786(8)
2.9	-0.0661(10)	-0.0665(10)	-0.0678(8)	-0.0689(7)	-0.0702(7)
3.4	-0.0595(10)	-0.0599(9)	-0.0611(8)	-0.0622(7)	-0.0634(6)
4.0	-0.0531(9)	-0.0535(8)	-0.0546(7)	-0.0557(6)	-0.0570(6)
4.8	-0.0464(8)	-0.0468(8)	-0.0478(7)	-0.0488(6)	-0.0501(5)

TABLE XX. Decay matrix elements at  $\beta = 2.187$ .

	$K=0.1343$	$K=0.1357$	$K=0.1367$	$K=0.1377$	$K=0.1383$
$aM_0$			$a^{3/2}(f\sqrt{M})^{(0)}$		
2.4	0.418(7)	0.430(8)	0.448(7)	0.466(6)	0.493(6)
2.9	0.435(8)	0.448(8)	0.467(7)	0.486(7)	0.514(7)
3.4	0.450(8)	0.463(9)	0.483(8)	0.502(7)	0.532(7)
4.0	0.465(9)	0.478(10)	0.499(9)	0.519(8)	0.549(8)
4.8	0.482(9)	0.495(11)	0.516(9)	0.537(9)	0.568(9)
$aM_0$			$a^{3/2}(f\sqrt{M})^{(1)}$		
2.4	-0.0543(13)	-0.0549(11)	-0.0567(11)	-0.0580(10)	-0.0598(9)
2.9	-0.0480(12)	-0.0486(10)	-0.0500(10)	-0.0513(9)	-0.0530(8)
3.4	-0.0432(11)	-0.0437(9)	-0.0447(8)	-0.0459(9)	-0.0475(8)
4.0	-0.0386(11)	-0.0390(9)	-0.0399(7)	-0.0408(8)	-0.0423(7)
4.8	-0.0339(11)	-0.0342(9)	-0.0350(7)	-0.0356(8)	-0.0370(7)

TABLE XXI. Decay matrix elements at  $\beta = 2.281$ .

	$K=0.1337$	$K=0.1349$	$K=0.1358$	$K=0.1368$	$K=0.1374$
$aM_0$			$a^{3/2}(f\sqrt{M})^{(0)}$		
2.4	0.359(8)	0.370(6)	0.389(6)	0.406(5)	0.428(5)
2.9	0.373(8)	0.385(7)	0.405(6)	0.423(5)	0.446(5)
3.4	0.384(9)	0.396(7)	0.418(6)	0.437(6)	0.462(6)
4.0	0.395(10)	0.408(8)	0.430(7)	0.451(6)	0.477(6)
4.8	0.407(11)	0.421(9)	0.444(7)	0.466(7)	0.493(7)
$aM_0$			$a^{3/2}(f\sqrt{M})^{(1)}$		
2.4	-0.0440(9)	-0.0449(8)	-0.0464(7)	-0.0477(6)	-0.0494(6)
2.9	-0.0389(9)	-0.0396(7)	-0.0410(6)	-0.0423(6)	-0.0438(6)
3.4	-0.0349(8)	-0.0356(7)	-0.0368(6)	-0.0380(6)	-0.0394(5)
4.0	-0.0311(8)	-0.0317(6)	-0.0328(6)	-0.0339(5)	-0.0352(5)
4.8	-0.0272(7)	-0.0277(6)	-0.0287(5)	-0.0296(5)	-0.0309(5)

TABLE XXII. Decay matrix elements at  $\beta = 2.334$ .

	$K = 0.1329$	$K = 0.1337$	$K = 0.1344$	$K = 0.1351$	$K = 0.1353$
$aM_0$			$a^{3/2}(f\sqrt{M})^{(0)}$		
2.4	0.221(3)	0.224(3)	0.235(2)	0.247(2)	0.261(2)
2.6	0.224(3)	0.227(3)	0.238(2)	0.251(2)	0.264(2)
2.9	0.228(3)	0.231(3)	0.243(2)	0.255(2)	0.269(2)
3.2	0.231(3)	0.234(3)	0.246(2)	0.259(2)	0.274(2)
3.5	0.234(3)	0.237(3)	0.250(3)	0.263(2)	0.277(2)
$aM_0$			$a^{3/2}(f\sqrt{M})^{(1)}$		
2.4	-0.0225(4)	-0.0227(3)	-0.0236(3)	-0.0245(3)	-0.0256(2)
2.6	-0.0213(3)	-0.0215(3)	-0.0223(3)	-0.0232(3)	-0.0242(2)
2.9	-0.0197(3)	-0.0199(3)	-0.0207(3)	-0.0215(2)	-0.0225(2)
3.2	-0.0184(3)	-0.0185(3)	-0.0193(2)	-0.0200(2)	-0.0209(2)
3.5	-0.0172(3)	-0.0173(3)	-0.0180(2)	-0.0188(2)	-0.0196(2)

TABLE XXIII. Decay matrix elements at  $\beta = 2.575$ .



- 
- [1] S. Hashimoto, in *Proceedings of the International Symposium on Lattice Field Theory*, Pisa, Italy, June 29–July 3, 1999, Nucl. Phys. B (Proc. Suppl.) **83-84** (2000) 3.
- [2] C. Bernard, in *Proceedings of the International Symposium on Lattice Field Theory*, Bangalore, India, August 17–22, 2000, Nucl. Phys. B (Proc. Suppl.) **94** (2001) 159.
- [3] A.X. El-Khadra, A.S. Kronfeld and P.B. Mackenzie, Phys. Rev. D55 (1997) 3933.
- [4] B.A. Thacker and G.P. Lepage, Phys. Rev. D43 (1991) 196; G.P. Lepage *et al.*, Phys. Rev. D46 (1992) 4052.
- [5] A. Ali Khan *et al.* (CP-PACS Collaboration), hep-lat/0010009.
- [6] S. Collins, C.T.H. Davies, U.M. Heller, A. Ali Khan, J. Shigemitsu, J. Sloan and C. Morningstar Phys. Rev. D60 (1999) 074504.
- [7] C. Bernard *et al.* (MILC Collaboration), Phys. Rev. Lett. 81 (1998) 4812; in *Proceedings of the International Symposium on Lattice Field Theory*, Pisa, Italy, June 29–July 3, 1999, Nucl. Phys. B (Proc. Suppl.) **83-84** (2000) 289; in *Proceedings of the International Symposium on Lattice Field Theory*, Bangalore, India, August 17–22, 2000, Nucl. Phys. B (Proc. Suppl.) **94** (2001) 346.
- [8] Y. Iwasaki, Nucl. Phys. **B258** 141 (1985); University of Tsukuba Report No. UTHEP-118, 1983.
- [9] B. Sheikholeslami and R. Wohlert, Nucl. Phys. **B259** 572 (1985).
- [10] R. Burkhalter, in *Proceedings of the International Symposium on Lattice Field Theory*, Boulder, USA, 13–18 July 1998, Nucl. Phys. (Proc. Suppl.) **73** (1999) 3.
- [11] CP-PACS Collaboration, A. Ali Khan *et al.*, Phys. Rev. Lett. 85 (2000) 4674.
- [12] CP-PACS Collaboration, A. Ali Khan *et al.*, in preparation.
- [13] K.-I. Ishikawa, H. Matsufuru, T. Onogi, N. Yamada and S. Hashimoto, Phys. Rev. D56 (1997) 7028.
- [14] A. Ali Khan, S. Collins, C.T.H. Davies, C. Morningstar, J. Shigemitsu and J. Sloan, Phys. Lett. B427 (1998) 132.
- [15] JLQCD Collaboration, K.-I. Ishikawa *et al.*, Phys. Rev. D61 (2000) 074501.
- [16] C.T.H. Davies, K. Hornbostel, A. Langnau, G.P. Lepage, A. Lidsey, J. Shigemitsu and J. Sloan, Phys. Rev. D50 (1994) 6963.
- [17] K.-I. Ishikawa, T. Onogi and N. Yamada, in *Proceedings of the International Symposium on Lattice Field Theory*, Pisa, Italy, July 1999, Nucl. Phys. (Proc. Suppl.) **83-84** (2000) 301.
- [18] C.J. Morningstar and J. Shigemitsu, Phys. Rev. D57 (1998) 6741.
- [19] CP-PACS Collaboration, T. Manke *et al.*, Phys. Rev. D62 (2000) 114508.
- [20] A. Ali Khan, T. Bhattacharya, S. Collins, C.T.H. Davies, R. Gupta, C. Morningstar, J. Shigemitsu and J. Sloan, Phys. Rev. D62 (2000) 054505.
- [21] J. Hein, S. Collins, C.T.H. Davies, A. Ali Khan, H. Newton, C. Morningstar, J. Shigemitsu and J. Sloan, Phys. Rev. D62 (2000) 074503.
- [22] G.P. Lepage and P. Mackenzie, Phys. Rev. D48 (1993) 2250.
- [23] C.T.H. Davies, K. Hornbostel, G.P. Lepage, A. Lidsey, P. McCallum, J. Shigemitsu and J. Sloan, Phys. Rev. D58 (1998) 054505.
- [24] S. Collins, C.T.H. Davies, J. Hein, G.P. Lepage, C.J. Morningstar, J. Shigemitsu, and J. Sloan, Phys. Rev. D63 (2001) 034505.

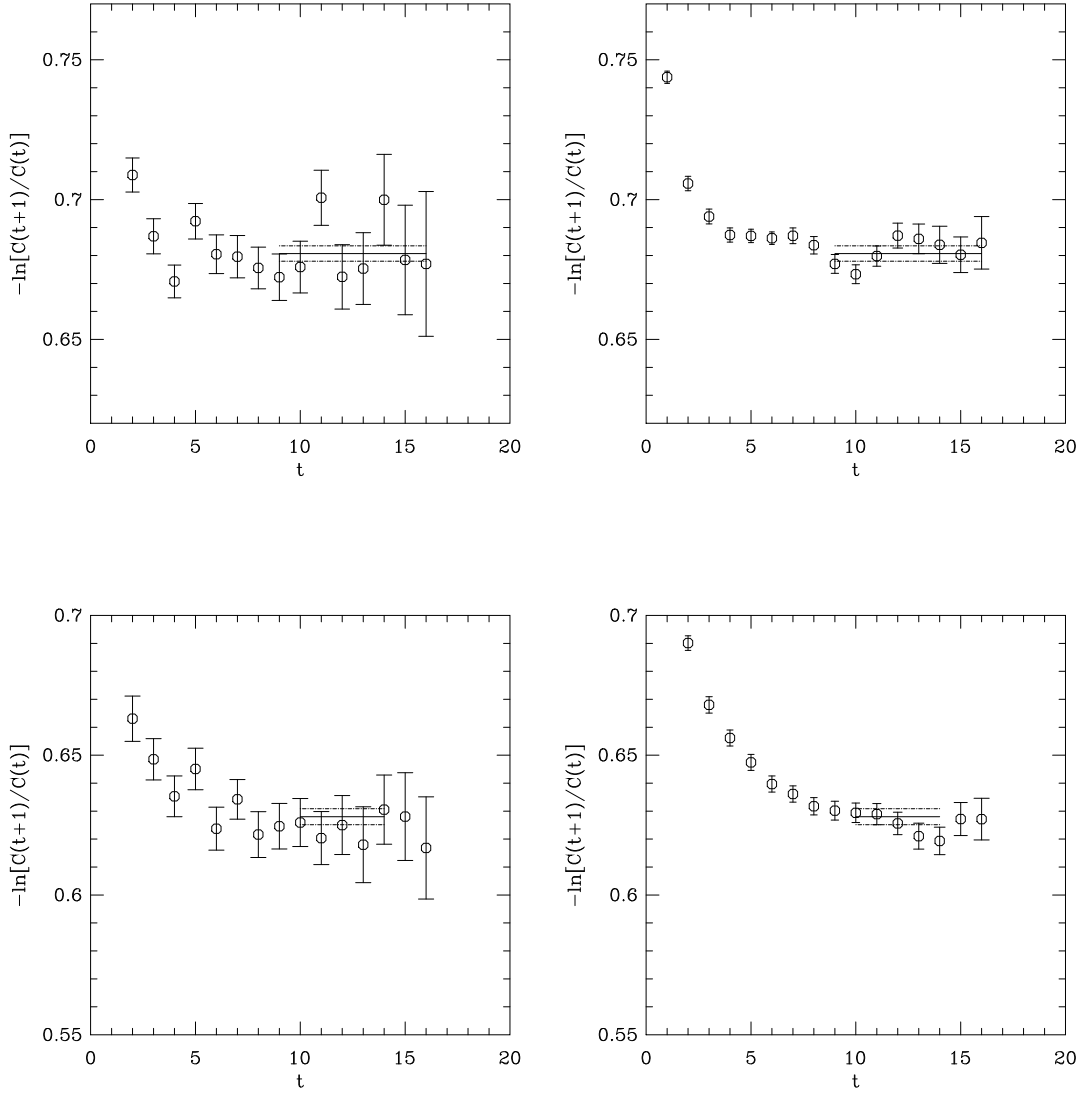


FIG. 1. Upper panels show effective mass of  $C_{SS}$  (left) and  $C_{SL}^{(0)}$  (right) in full QCD at  $\beta = 1.95$ ,  $K_{sea} = 0.1410$ ,  $K_{val} = 0.1390$ , and  $aM_0 = 4.0$ . Lower panels are for quenched QCD at  $\beta = 2.334$  for  $K = 0.1349$  and  $aM_0 = 4.0$ . Solid and dashed lines show fit results and one standard deviation error bands.

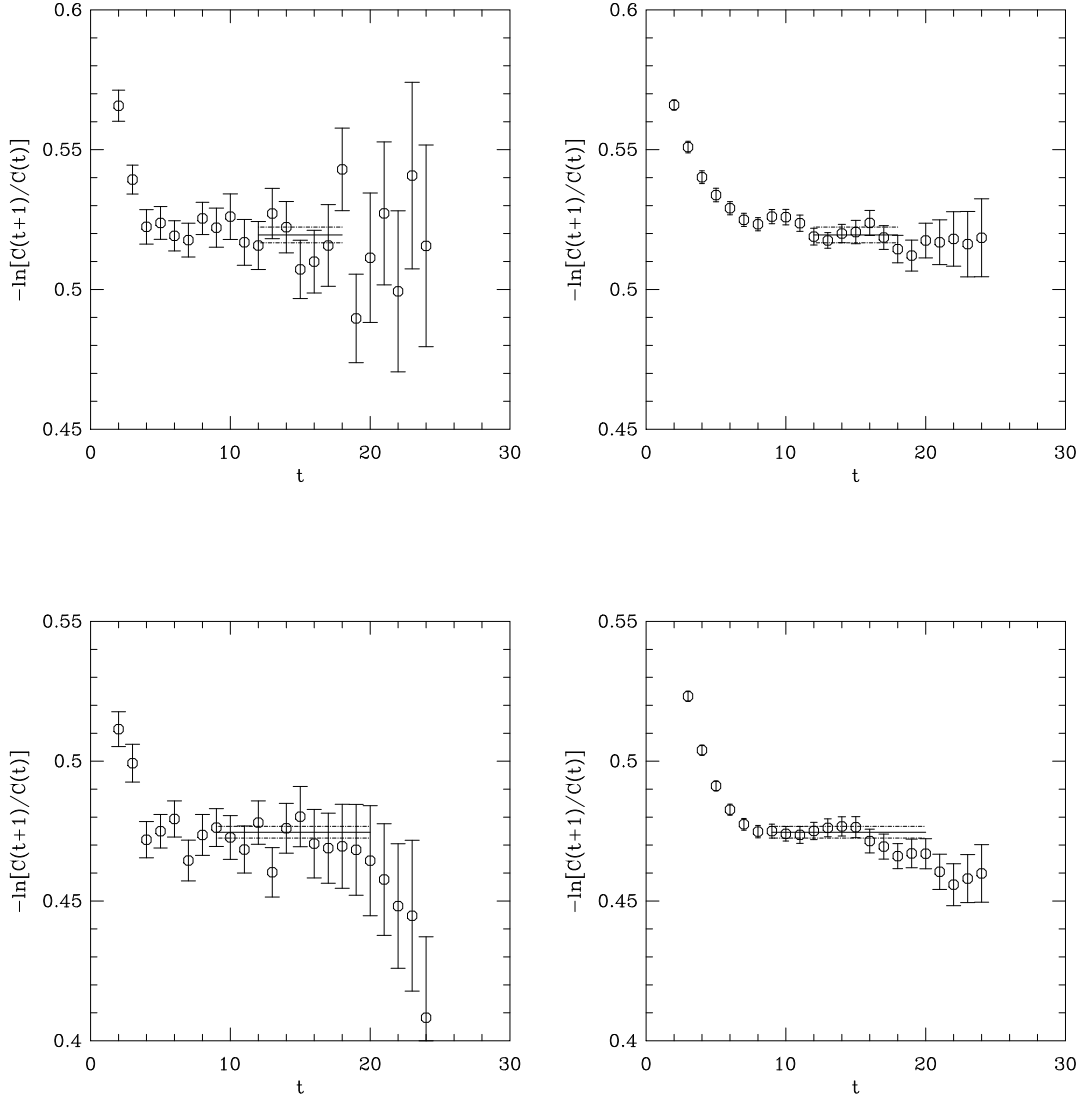


FIG. 2. Upper panels show effective mass  $\cdot$  of  $C_{SS}$  (left) and  $C_{SL}^{(0)}$  (right) in full QCD at  $\beta = 2.1$ ,  $K_{sea} = 0.1382$ ,  $K_{val} = 0.1374$ , and  $aM_0 = 2.9$ . Lower panels are for quenched QCD at  $\beta = 2.575$ ,  $K_{val} = 0.1374$ , and  $aM_0 = 2.9$ .

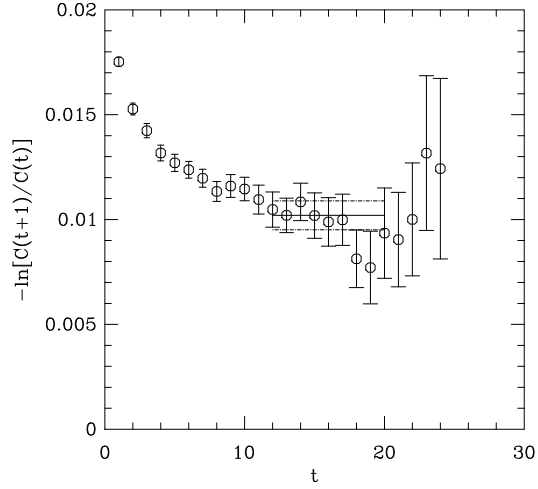


FIG. 3. Effective mass plot of the ratio of correlators at  $p = 2\pi/L$  and at  $p = 0$  for  $\beta = 2.1$ ,  $K_{sea} = 0.1382$ . Valence quark masses correspond to  $K_{val} = 0.1374$  and  $aM_0 = 2.9$ .

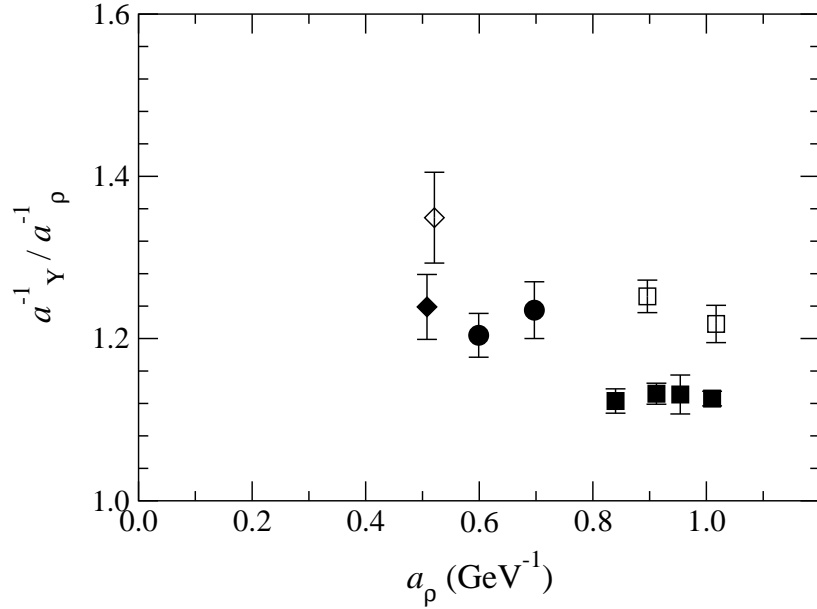


FIG. 4. Ratio of inverse lattice spacings from  $\Upsilon(1P - 1S)$  and  $m_\rho$  for full (filled symbols) and quenched (open symbols) QCD. Our results for  $N_f = 2$  (partially quenched) lattices are denoted by filled squares ( $\beta = 1.95$ ) and by filled circles ( $\beta = 2.1$ ) [19]. The open and filled diamonds denote a quenched [14,23] and partially quenched [6] result respectively, for the plaquette gauge action. Error bars are purely statistical.

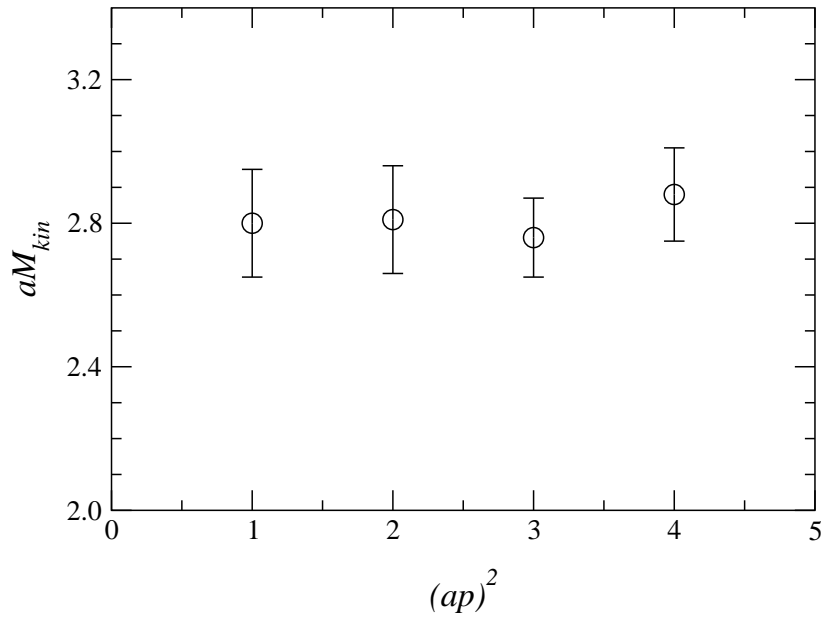
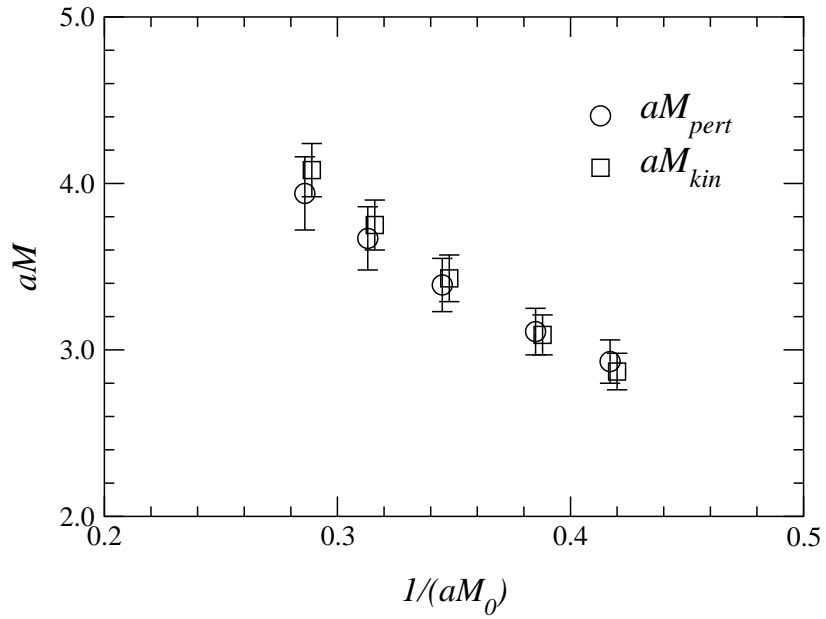


FIG. 5. Kinetic mass at  $\beta = 2.575$ , extracted from Eq. 18, in lattice units, as a function of the momentum  $p^2$  in units of  $(2\pi/L)^2$ . The quark mass parameters are  $K_{sea} = 0.1344$  and  $aM_0 = 2.6$ .



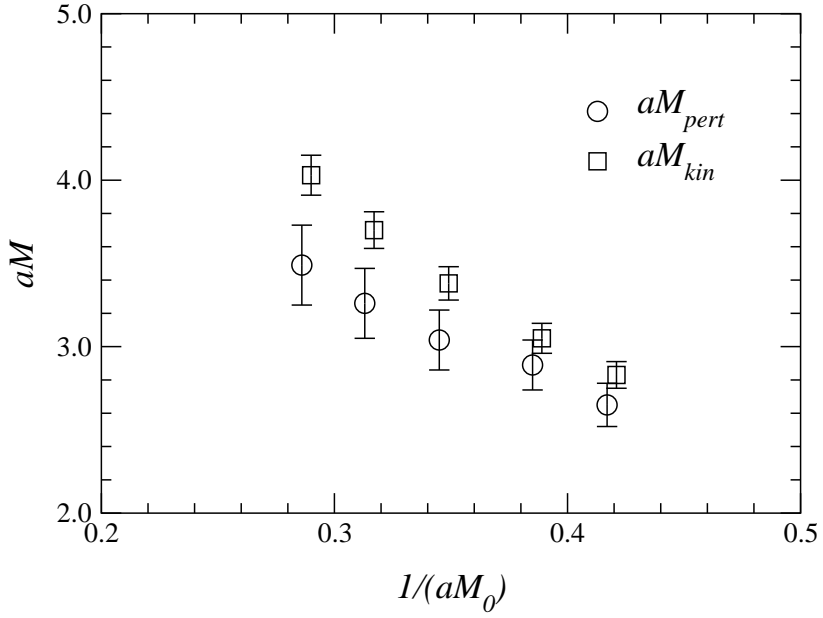


FIG. 6. Comparison of kinetic mass (circles) and mass using perturbative shifts (squares) in full QCD at  $\beta = 2.1$ ,  $K_{sea} = 0.1382$  and  $K_{val} = 0.1374$  (top panel), and in quenched QCD at  $\beta = 2.575$ ,  $K = 0.1344$  (bottom panel).

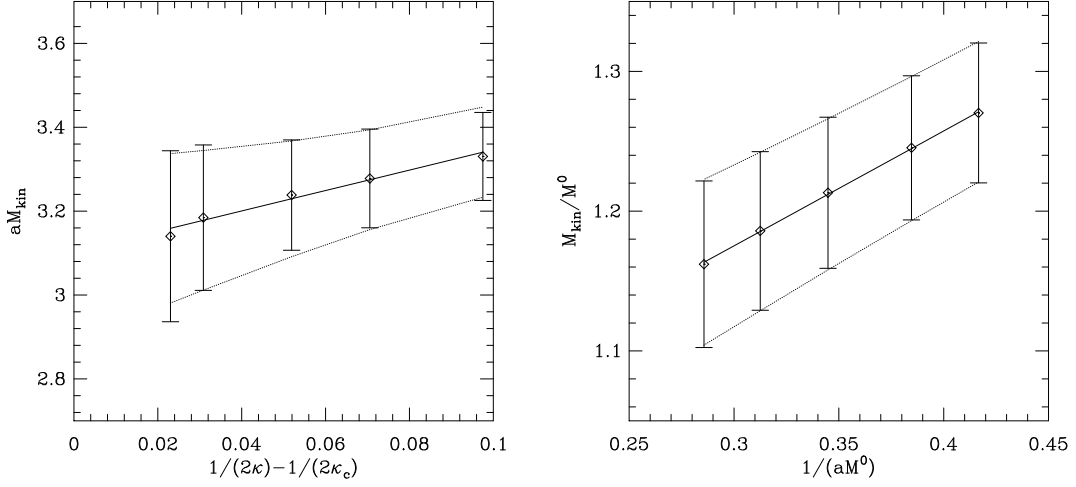


FIG. 7. Kinetic meson mass for the parameter values  $\beta = 2.1$ ,  $K_{sea} = 0.1374$  in full QCD. Left panel shows a fit of  $M_{kin}$  as a function of the light quark mass for  $aM_0 = 2.6$ , which is close to  $M_{0b}$ . Right panel shows a fit in the heavy quark mass with the light quark mass interpolated to the strange quark mass. Solid lines denote the fits and dashed lines the error.

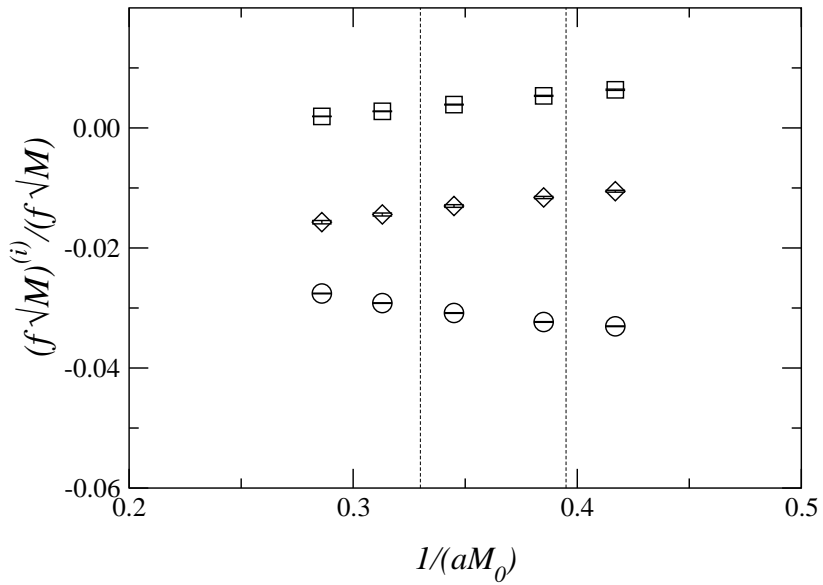
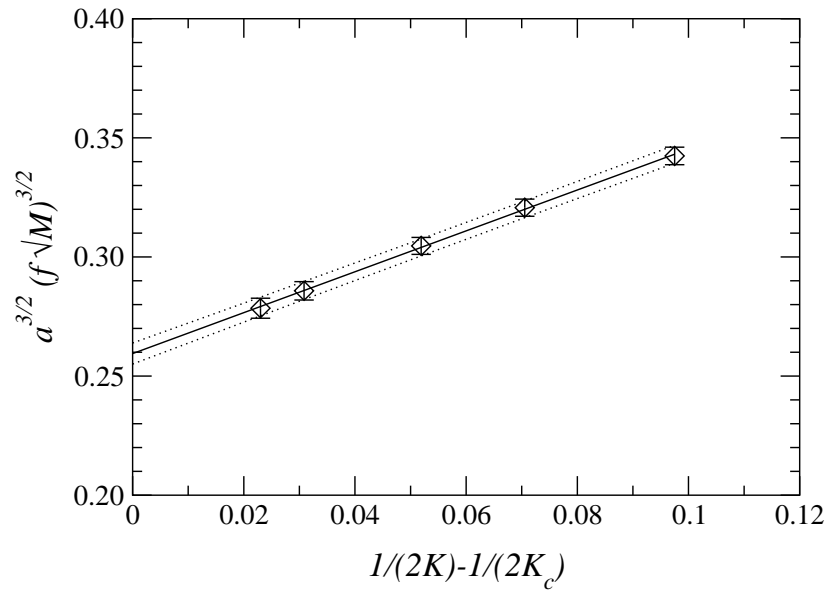


FIG. 8. Relative size of the one-loop corrections to the current matrix elements in full QCD. Circles denote  $\alpha_s \rho_0 (f\sqrt{M})^{(0)}/(f\sqrt{M})$ , squares stand for  $\alpha_s \rho_1 (f\sqrt{M})^{(1)}/(f\sqrt{M})$ , and diamonds give  $\alpha_s \rho_2 (f\sqrt{M})^{(2)}/(f\sqrt{M})$ . The two vertical lines is a band to indicate the position of the bare  $b$  quark mass. Parameter values are  $\beta = 2.1$ ,  $K_{sea} = K_{val} = 0.1382$ .



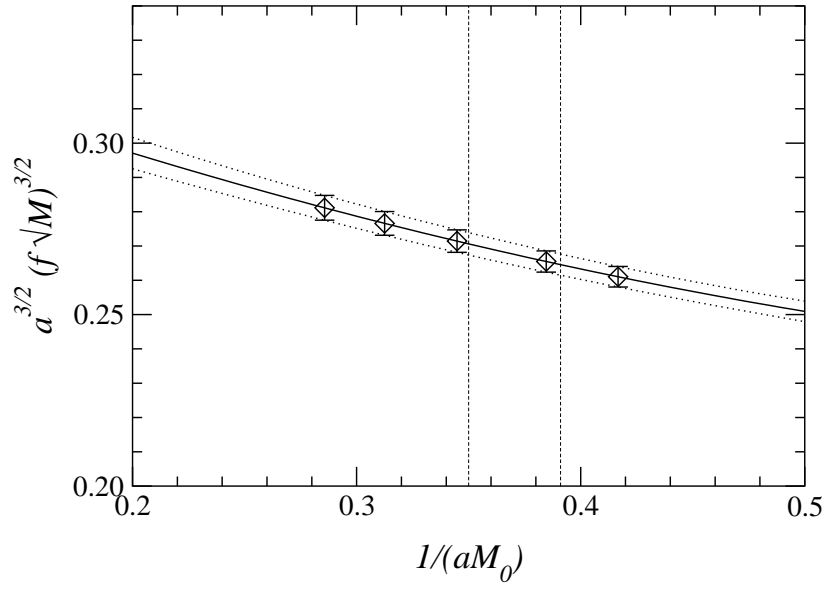


FIG. 9. Decay matrix elements for the parameter values  $\beta = 2.1$ ,  $K_{sea} = 0.1374$ . Top panel shows a fit of  $(f\sqrt{M})^{(0)}$  as a function of the light quark mass for  $aM_0 = 2.6$ , which is close to  $M_{0b}$ . Bottom panel shows a fit of  $(f\sqrt{M})$  in the heavy quark mass with the light quark mass interpolated to the strange quark mass. Solid curves denote the fits and dotted lines the error. The vertical lines in the figure on the bottom give the error bounds of  $aM_{0b}$ .

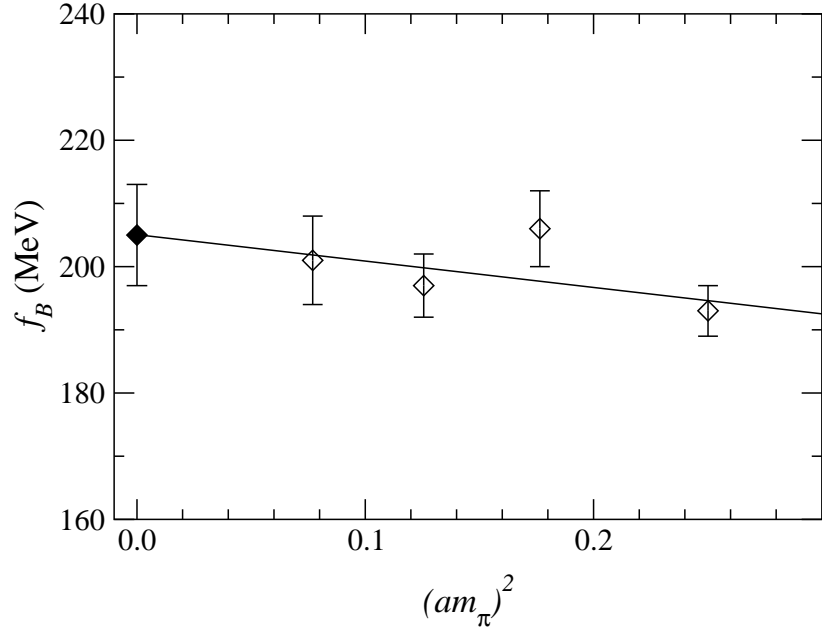


FIG. 10. Decay constant at  $\beta = 2.1$  as a function of the sea quark mass. Open symbols denote the partially quenched results, the solid line the fit in  $(am_\pi)^2$ , and the filled symbol the value in the chiral limit of the sea quark mass.



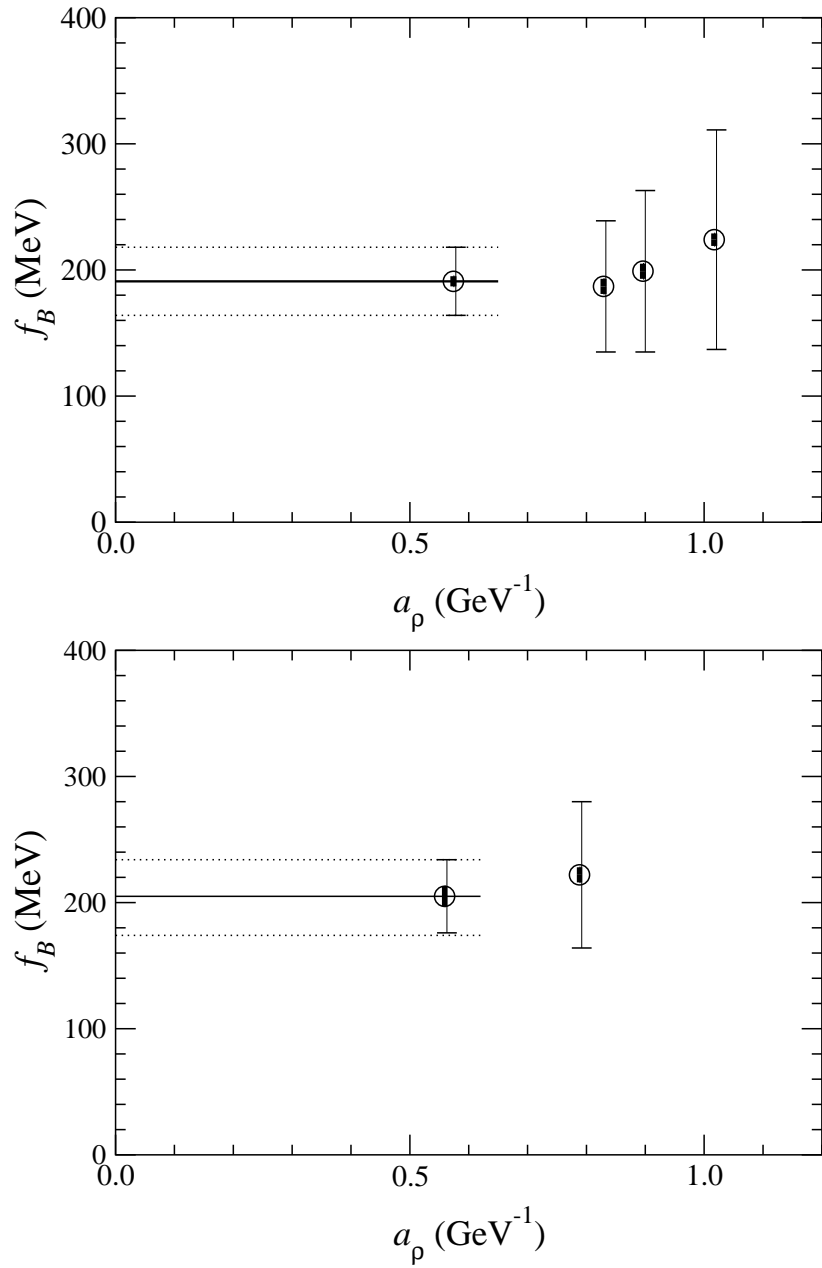


FIG. 11.  $f_B$  as a function of the lattice spacing in quenched QCD (top) and full QCD (bottom). Thick error bars denote statistical, thin error bars, systematic errors. The solid horizontal line shows the final estimate for  $f_B$  taken from the finest lattice, the dashed horizontal lines, the error (statistical and systematic added in quadrature) on this estimate.

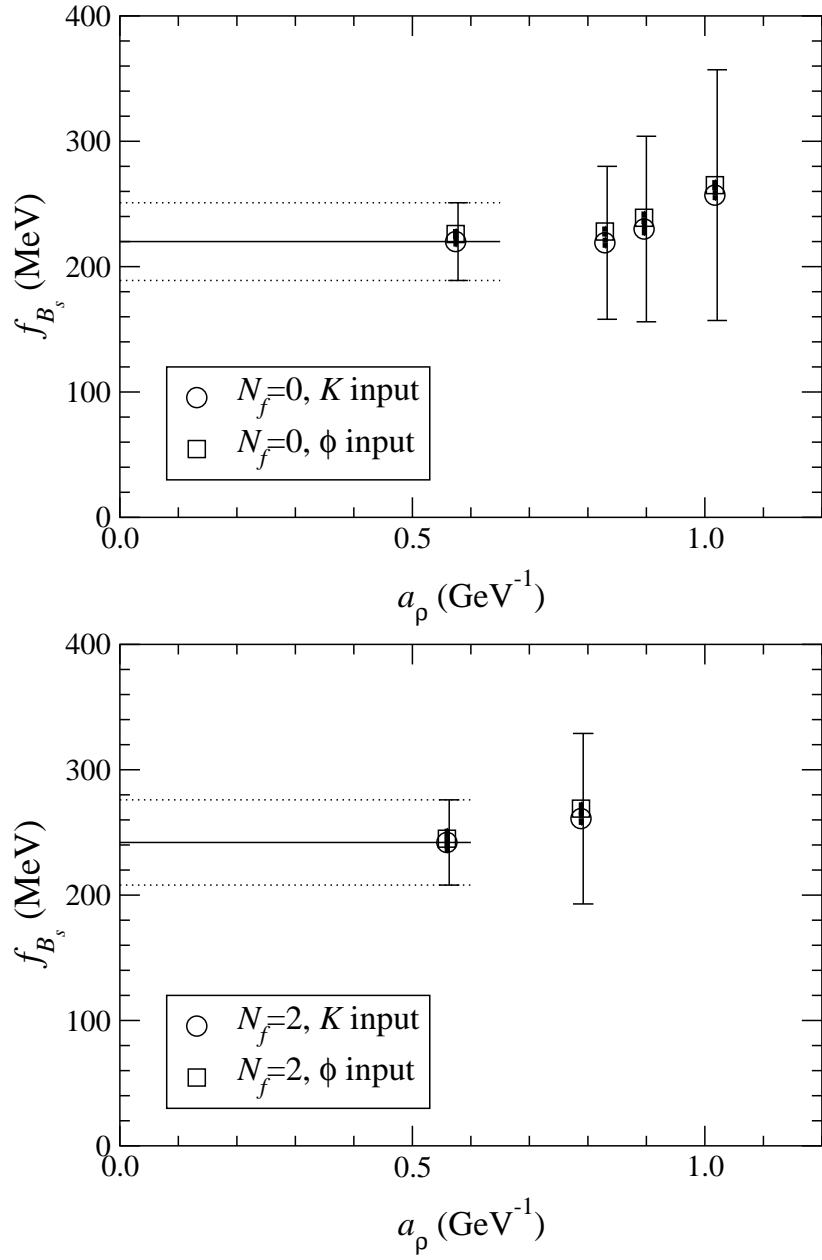


FIG. 12.  $f_{B_s}$  as a function of the lattice spacing in quenched QCD (top) and full QCD (bottom). Thick error bars denote statistical errors, thin ones, systematic errors. The solid horizontal line shows the final estimate for  $f_{B_s}$  taken from the result on the finest lattice, the dashed horizontal lines, the error on this estimate.

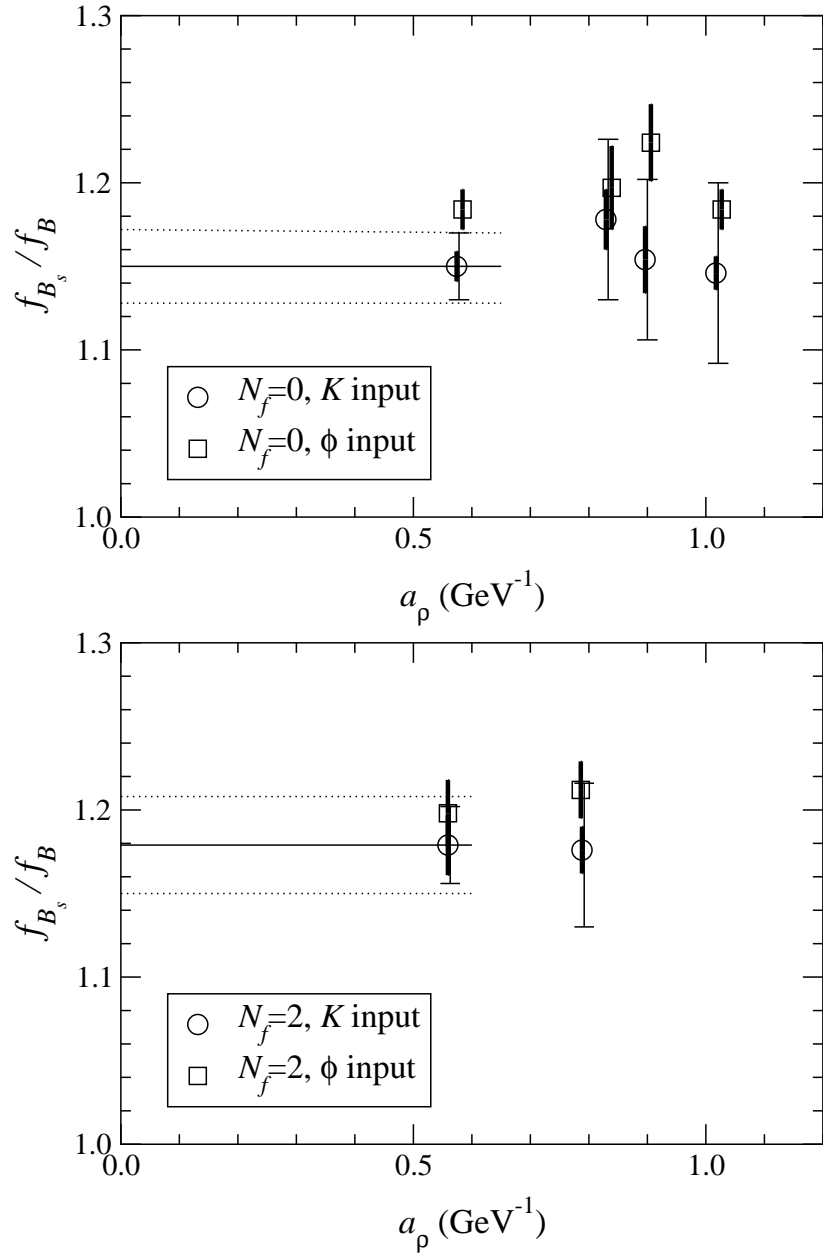


FIG. 13.  $f_{B_s}/f_B$  as a function of the lattice spacing in quenched QCD (top) and full QCD (bottom). Thick error bars denote statistical errors, thin ones, systematic errors. The solid horizontal line shows the final estimate for  $f_{B_s}/f_B$  taken from the finest lattice, the dashed horizontal lines, the error on this estimate.

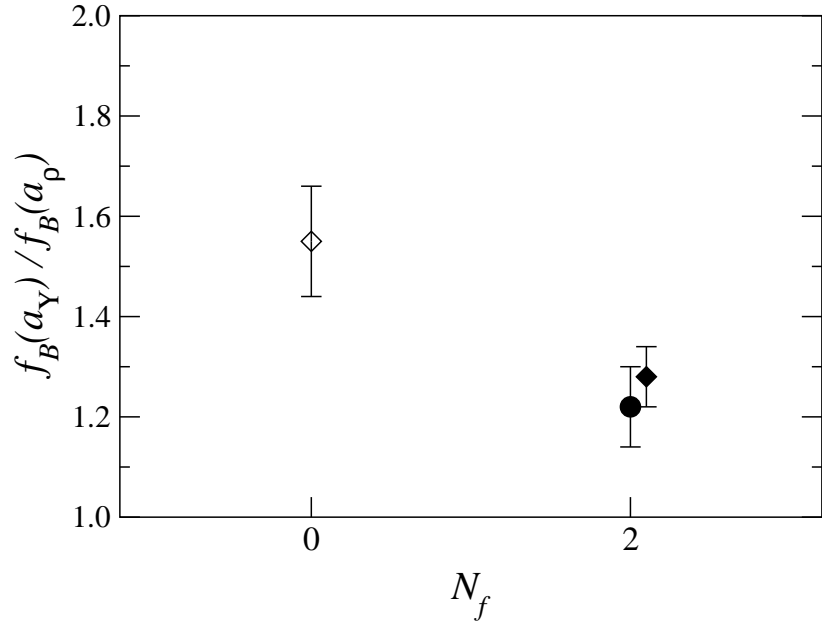


FIG. 14. Ratio of decay constants determined with  $a_\Upsilon$  and  $a_\rho$  for quenched ( $N_f = 0$ ) and partially quenched ( $N_f = 2$ ) QCD. Filled circle is our results, while filled diamond is from [6]. The quenched data (open diamond) has been obtained reanalyzing the results from [14] using lattice spacings from the  $\Upsilon$ .

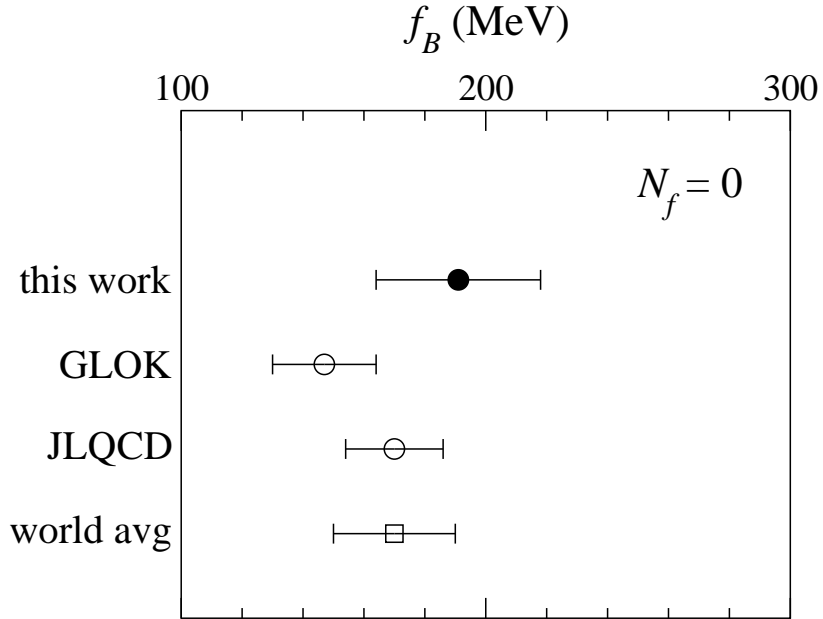


FIG. 15. Comparison of quenched results for  $f_B$  from NRQCD. The filled circle denotes the quenched result quoted in this paper, while two open circles show results from other recent NRQCD studies [14] and [15]. The open square stands for the quenched world average quoted in [1]. Errors include statistical and systematic errors combined in quadrature.

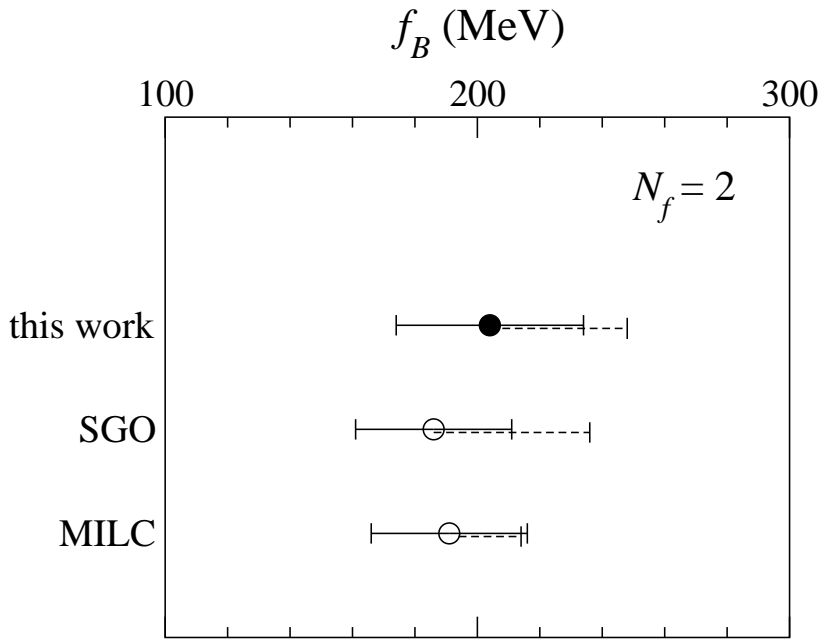


FIG. 16. Comparison of results for  $f_B$  in  $N_f = 2$  QCD. The filled circle denotes the result quoted in this paper for  $N_f = 2$ , the two open circles stand for the results from [6] and [7]. Solid error bars include statistical and systematic errors combined in quadrature. The uncertainty from setting the lattice spacing from light physics quantities or  $\Upsilon$  spectroscopy is shown separately in dotted lines.